




## Article

# Interaction Network Provides Clues on the Role of BCAR1 in Cellular Response to Changes in Gravity

Johann Bauer <sup>1,\*</sup>, Erich Gombocz <sup>2</sup>, Herbert Schulz <sup>3</sup>, Jens Hauslage <sup>4</sup> and Daniela Grimm <sup>3,5</sup><sup>1</sup> SiHaTho GmbH, Postfach 1106, 35201 Biedenkopf, Germany<sup>2</sup> Melissa Informatics, 22382 Avenida Empresa, Rancho Sana Margarita, CA 92688, USA; egombocz@ix.netcom.com<sup>3</sup> Department of Microgravity and Translational Regenerative Medicine, Clinic for Plastic, Aesthetic and Hand Surgery, Otto-von-Guericke University, 39106 Magdeburg, Germany; Herbert.Schulz@med.ovgu.de (H.S.); dgg@biomed.au.dk (D.G.)<sup>4</sup> DLR, Institut für Luft- und Raumfahrtmedizin, Linder Höhe, 51147 Köln, Germany; Jens.Hauslage@dlr.de<sup>5</sup> Department of Biomedicine, Aarhus University, Ole Worms Allé 4, DK-8000 Aarhus, Denmark

\* Correspondence: jbauer@sihatho.de

**Abstract:** When culturing cells in space or under altered gravity conditions on Earth to investigate the impact of gravity, their adhesion and organoid formation capabilities change. In search of a target where the alteration of gravity force could have this impact, we investigated p130cas/BCAR1 and its interactions more thoroughly, particularly as its activity is sensitive to applied forces. This protein is well characterized regarding its role in growth stimulation and adhesion processes. To better understand BCAR1's force-dependent scaffolding of other proteins, we studied its interactions with proteins we had detected by proteome analyses of MCF-7 breast cancer and FTC-133 thyroid cancer cells, which are both sensitive to exposure to microgravity and express BCAR1. Using linked open data resources and our experiments, we collected comprehensive information to establish a semantic knowledgebase and analyzed identified proteins belonging to signaling pathways and their networks. The results show that the force-dependent phosphorylation and scaffolding of BCAR1 influence the structure, function, and degradation of intracellular proteins as well as the growth, adhesion and apoptosis of cells similarly to exposure of whole cells to altered gravity. As BCAR1 evidently plays a significant role in cell responses to gravity changes, this study reveals a clear path to future research performing phosphorylation experiments on BCAR1.

**Keywords:** knowledge explorer; pathway studio; mass spectrometry; post-translational modification; network analysis; SPARQL



**Citation:** Bauer, J.; Gombocz, E.; Schulz, H.; Hauslage, J.; Grimm, D. Interaction Network Provides Clues on the Role of BCAR1 in Cellular Response to Changes in Gravity. *Computation* **2021**, *9*, 81. <https://doi.org/10.3390/computation9080081>

Academic Editor: Rainer Breitling

Received: 30 June 2021

Accepted: 20 July 2021

Published: 23 July 2021

**Publisher's Note:** MDPI stays neutral with regard to jurisdictional claims in published maps and institutional affiliations.



**Copyright:** © 2021 by the authors. Licensee MDPI, Basel, Switzerland. This article is an open access article distributed under the terms and conditions of the Creative Commons Attribution (CC BY) license (<https://creativecommons.org/licenses/by/4.0/>).

## 1. Introduction

When monolayers of tissue cells are cultured on a random positioning machine (RPM) or during spaceflight, the gravity force experienced by the cells is altered in that it pulls the cells of a monolayer constantly towards the center of the Earth. Under this condition of prevented sedimentation, several cellular features change in comparison to control cells cultured under normal laboratory conditions [1–3]. To extend our knowledge about the cellular adjustment to prevented sedimentation, we investigated the role of BCAR1 (breast cancer anti-estrogen resistance protein 1) also known as p130cas (CRK-associated substrate), because this protein is known to be a primary sensor of forces [4]. According to current knowledge, forces pulling the C- and the N-terminal ends of BCAR1 apart effect changes of its phosphorylation status [5].

Phosphorylation is a well-studied reversible post-translational modification (PTM) of many proteins [6]. It is catalyzed by protein kinases (PK) and is reversed by protein phosphatases (PPs). However, the extent of phosphorylation of particular proteins within cells does not only depend on the content and/or activity of cognate PKs or PPs or both [7].

The consensus motif (CM) of a target protein must also be so accessible that it can correctly be positioned within the catalytic site of a kinase [8,9]. This correct positioning depends on parameters [10] such as the three-dimensional order and the side chain orientation of amino acids surrounding the target amino acid [11]. The CMs' accessibility may be changed by factors such as the docking of low- or high-molecular-weight ligands at the protein to be modified [12,13] as well as by the binding of target proteins to components of the cell membrane [14,15]. Furthermore, an initial phosphorylation influences subsequent phosphorylation steps [16]. In addition, forces which stretch the amino acid chains of specific domains, called intrinsically disordered domains, of target proteins modulate the accessibility of target CMs. This has been proven for several proteins, such as the cytoplasmic domain of PECAM-1 [17], the beta-catenin/E-cadherin complex [18] and BCAR1 [4,5].

BCAR1 is an adapter protein, which links cell–cell and cell–matrix adhesion to an extended signaling network [19]. It consists of 870 amino acids, which form five domains: an N-terminal SH3 homology domain, followed towards the C-terminus by a proline-rich region, a Substrate Domain (SD), a serine-rich domain, a Substrate-Binding Domain (SBD) and a Focal Adhesion Targeting Domain which docks BCAR1 at a focal adhesion complex [5,20]. The three-dimensional structures of the N-terminal SH3 homology domain and of the C-terminal Focal Adhesion Targeting domain have been resolved at 1.1 and 2.5 Angström resolutions [20,21]. The three domains in between are functionally well characterized as described below. BCAR1 generates signals via binding different effector proteins. The selection of binding and interaction partners is influenced by the protein's status of phosphorylation and conformation [19], which depends at least partially on the traction forces extending its three-dimensional conformation. In respect to the action of forces, the most interesting part of BCAR1 is the so-called Substrate Domain (SD). This domain has an intrinsically disordered conformation, which includes 15 tyrosine phosphorylation sites (YxxP) [22]. If the domain's conformation is extended with minimal force, the phosphorylation sites become accessible for Src family kinases [23,24]. The forces to stretch the domain may be generated in vivo by the cytoskeletal actin myosin system and the focal adhesion system linked to the N-terminal end via the SH3 domain and to the C-terminal end via the C-terminal Focal Adhesion Targeting domain [4,25–27]. The force application to BCAR1 influences cell adhesion, cytoskeletal organization and growth factor receptors' signaling [28–30].

It has been described that BCAR1 gene expression is upregulated in multipotent mesenchymal stromal cells under microgravity [31] and is regulated in endothelial cells [32] and MCF7 cells [33]. Furthermore, a transient upregulation in MDA-MB-231 breast cancer cells has been reported [34]. Therefore, we wanted to see whether gravity forces could also influence BCAR1 activity on a protein level, particularly as recent proteome analysis suggested an influence of gravity on the accumulation of BCAR1 in MCF-7 and in FTC-133 cancer cells [35,36]. Hence, we collected information about the biochemical effects of force-dependent changes of BCAR1 phosphorylation and complex formation described in literature and compared the results with the behavior of cells exposed to microgravity. After identifying the proteins known to interact with BCAR1 and detected in MCF-7 or FTC-133 cancer cells by our proteome analysis [35,36], we composed two exemplary sets of data. Using harmonized import mapping via Knowledge Explorer (KE), both types of data were aggregated in a semantic knowledgebase [37]. Using this base, we established protein interaction networks that show the impact of BCAR1 interaction activities on cell physiology and signal transduction.

## 2. Results

### 2.1. Selection of Proteins

To study BCAR1 scaffolding activities, we created an overview on proteins capable of interacting with BCAR1. Applying STRING, we recorded 50 proteins, co-mentioned with BCAR1 in entries of the literature database Medline. The result was complemented

by another 31 proteins obtained through searches in the dbPTM database as well as by evaluating the references [5,20]. To examine protein interactions and signal transduction, which can happen in a distinct kind of cells, we separately analyzed those of the proteins which we detected in recent proteome analyses of MCF-7 breast cancer cells [35] and of FTC-133 thyroid cancer cells [36], respectively. Data from MCF-7 cells were of interest because the role of BCAR1 in these cells is well characterized [38,39]. For comparison purposes, FTC-133-derived data were opposed. The FTC-133 cell line was isolated from a man suffering thyroid tumors [40]. It is a fast-growing cell line with a mutated P53 gene [41] and responds very quickly to exposure to simulated microgravity [42]. Furthermore, we detected BCAR1 protein as well as BCAR1 gene expression in this cell line in previous studies [36,43]. For subsequent network analyses, 81 proteins potentially interacting with BCAR1 were matched against the 5924 proteins found in the proteome analysis of FTC-133 cells and against the 6968 proteins found in the analysis of MCF-7 cells [35,36].

As shown in Table 1, 39 of the BCAR1-related proteins had been detected in proteome analyses of MCF-7 and of FTC-133 cells. Another 12 and 8 proteins were found only in the MCF-7 (marked by \*) or FTC-133 cells (marked by \*\*), respectively. Independently of their source, these proteins had different activities. A total of 25 proteins were enzymes, including 12 kinases and 6 phosphatases (Figure 1). Another 24 are proteins which either bind to different other proteins or adapt other proteins within complexes. Besides BCAR1, six other proteins were found with intrinsically disordered domains, which change their conformation upon the impact of low forces [22,23]. Three of the six proteins were detected in MCF-7 cells and another three in FTC-133 cells (Figure 1).

**Table 1.** List of selected proteins. The selected proteins were detected in both cell lines or in MCF-7 cells only (marked by \*) or in FTC-133 cells only (marked by \*\*).

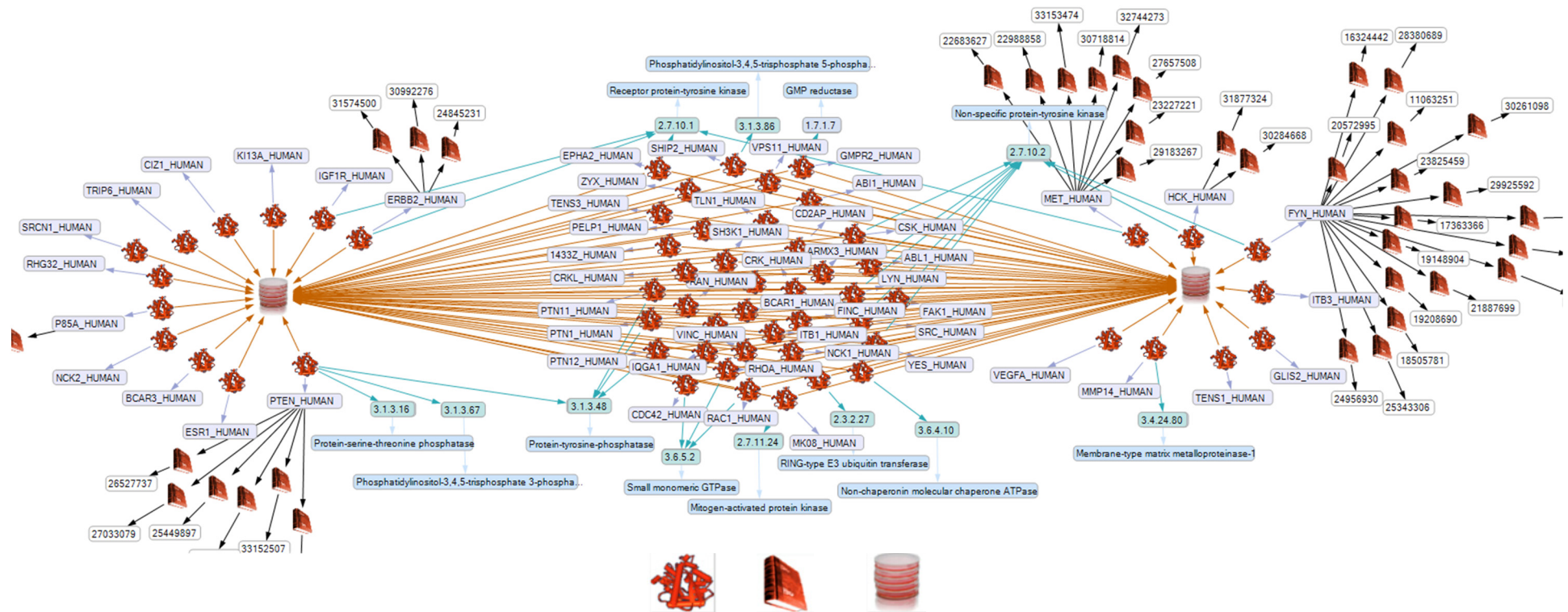
Entry	Gene Name	SwissProt Accession No.	Protein Name	Activity/Function
ABI1_HUMAN	<i>ABI1</i>	Q8IZP0	Abl interactor 1	Adapter
ABL1_HUMAN	<i>ABL1</i>	P00519	Tyrosine-protein kinase ABL1	Enzyme
RHG32_HUMAN	<i>ARHGAP32</i>	A7KAX9 *	Rho GTPase-activating protein 32	Adapter
ARMX3_HUMAN	<i>ARMCX3</i>	Q9UH62	Armadillo repeat-containing X-linked protein3	Binding protein
BCAR1_HUMAN	<i>BCAR1</i>	P56945	Breast cancer anti-estrogen resistance protein 1 or p130cas (CRK-associated substrate)	Binding protein
BCAR3_HUMAN	<i>BCAR3</i>	O75815 *	Breast cancer anti-estrogen resistance protein 3	Adapter
CBL_HUMAN	<i>CBL</i>	P22681	E3 ubiquitin-protein ligase CBL	Enzyme
CD2AP_HUMAN	<i>CD2AP</i>	Q9Y5K6	CD2-associated protein	Adapter
CDC42_HUMAN	<i>CDC42</i>	P60953	Cell division control protein 42 homolog	Enzyme
CIZ1_HUMAN	<i>CIZ1</i>	Q9ULV3 *	Cip1-interacting zinc finger protein	Binding protein
CRK_HUMAN	<i>CRK</i>	P46108	Adapter molecule crk	Adapter
CRKL_HUMAN	<i>CRKL</i>	P46109	Crk-like protein	Adapter
CSK_HUMAN)	<i>CSK</i>	P41240	Tyrosine-protein kinase CSK	Enzyme
EPHA2_HUMAN	<i>EPHA2</i>	P29317	Ephrin type-A receptor 2	Enzyme
ERBB2_HUMAN	<i>ERBB2</i>	P04626 *	Receptor tyrosine-protein kinase erbB-2	Enzyme

Table 1. Cont.

Entry	Gene Name	SwissProt Accession No.	Protein Name	Activity/Function
ESR1_HUMAN	<i>ESR1</i>	P03372 *	Estrogen receptor	Hormone receptor
FINC_HUMAN	<i>FN1</i>	P02751	Fibronectin	ECM protein
FYN_HUMAN	<i>FYN</i>	P06241 **	Tyrosine-protein kinase Fyn	Enzyme
GLIS2_HUMAN	<i>GLIS2</i>	Q9BZE0 **	Zinc finger protein GLIS2	Binding protein
GMPR2_HUMAN	<i>GMPR2</i>	Q9P2T1	GMP reductase 2	Enzyme
HCK_HUMAN	<i>HCK</i>	P08631 **	Tyrosine-protein kinase HCK	Enzyme
BIP_HUMAN	<i>HSPA5</i>	P11021	Endoplasmic reticulum chaperone BiP	Enzyme
IGF1R_HUMAN	<i>IGF1R</i>	P08069 *	Insulin-like growth factor 1 receptor	Enzyme
IQGA1_HUMAN	<i>IQGA1</i>	P46940	Ras GTPase-activating-like protein IQGAP1	Binding protein
ITAV_HUMAN	<i>ITGAV</i>	P06756	Integrin alpha-V	Binding protein
ITB1_HUMAN	<i>ITGB1</i>	P05556	Integrin beta-1	Binding protein
ITB3_HUMAN	<i>ITGB3</i>	P05106 **	Integrin beta-3	Binding protein
KI13A_HUMAN	<i>KIF13A</i>	Q9H1H9 *	Kinesin-like protein KIF13A	Motor protein
LYN_HUMAN	<i>LYN</i>	P07948	Tyrosine-protein kinase Lyn	Enzyme
MK08_HUMAN	<i>MAPK8</i>	P45983	Mitogen-activated protein kinase 8	Enzyme
MET_HUMAN	<i>MET</i>	P08581 **	Hepatocyte growth factor receptor	Enzyme
MMP14_HUMAN	<i>MMP14</i>	P50281 **	Matrix metalloproteinase-14	Enzyme
NCK1_HUMAN	<i>NCK1</i>	P16333	Cytoplasmic protein NCK1	Adapter
NCK2_HUMAN	<i>NCK2</i>	O43639 *	Cytoplasmic protein NCK2	Adapter
PELP1_HUMAN	<i>PELP1</i>	Q8IZL8	Proline-, glutamic acid- and leucine-rich protein 1	Binding protein
P85A_HUMAN	<i>PIK3R1</i>	P27986 *	Phosphatidylinositol 3-kinase regulatory subunit alpha	Adapter
PTEN_HUMAN	<i>PTEN</i>	P60484 *	Phosphatidylinositol 3,4,5-trisphosphate 3-phosphatase and dual-specificity protein phosphatase PTEN	Enzyme
FAK1_HUMAN	<i>PTK2</i>	Q05397	Focal adhesion kinase 1	Enzyme
PTN12_HUMAN	<i>PTN12</i>	Q05209	Tyrosine-protein phosphatase non-receptor type 12	Enzyme
PTN1_HUMAN	<i>PTPN1</i>	P18031	Tyrosine-protein phosphatase non-receptor type 1	Enzyme
PTN11_HUMAN	<i>PTPN11</i>	Q06124	Tyrosine-protein phosphatase non-receptor type 11	Enzyme
PAXI_HUMAN	<i>PXN</i>	P49023	Paxillin	Cytoskeletal protein
RAC1_HUMAN	<i>RAC1</i>	P63000	Ras-related C3 botulinum toxin substrate 1	Enzyme

Table 1. Cont.

Entry	Gene Name	SwissProt Accession No.	Protein Name	Activity/Function
RAN_HUMAN	<i>RAN</i>	P62826	GTP-binding nuclear protein Ran	Binding protein
RHOA_HUMAN	<i>RHOA</i>	P61586	Transforming protein RhoA	Enzyme
SH3K1_HUMAN	<i>SH3KBP1</i>	Q96B97	SH3 domain-containing kinase-binding protein 1	Adapter
SHIP2_HUMAN	<i>SHIP2</i>	O15357	Phosphatidylinositol 3,4,5-trisphosphate 5-phosphatase 2	Enzyme
SRC_HUMAN	<i>SRC</i>	P12931	Proto-oncogene tyrosine-protein kinase Src	Enzyme
SRCN1_HUMAN	<i>SRCN1</i>	Q9C0H9 *	SRC kinase signaling inhibitor 1	Inhibitor
TENS3_HUMAN	<i>TNS3</i>	Q68CZ2	Tensin-3	Cytoskeletal protein
TLN1_HUMAN	<i>TLN1</i>	Q9Y490	Talin-1	Cytoskeletal protein
TENS1_HUMAN	<i>TNS1</i>	Q9HBL0 **	Tensin-1	Cytoskeletal protein
TRIP6_HUMAN	<i>TRIP6</i>	Q15654 *	Thyroid receptor-interacting protein 6	Binding protein
VINC_HUMAN	<i>VCL</i>	P18206	Vinculin	Cytoskeletal protein
VEGFA_HUMAN	<i>VEGFA</i>	P15692 **	VEGFA	Growth factor
VPS11_HUMAN	<i>VPS11</i>	Q9H270	Vacuolar protein sorting-associated protein 11 homolog	Binding protein
YES_HUMAN	<i>YES1</i>	P07947	Tyrosine-protein kinase Yes	Enzyme
1433Z_HUMAN	<i>YWHAZ</i>	P63104	14-3-3 protein zeta/delta	Adapter
ZYX_HUMAN	<i>ZYX</i>	Q15942	Zyxin	Binding protein



**Figure 1.** Types of enzymes included in the list of selected proteins and related to BCAR1 from MCF-7 and FTC-133 cells. Proteins are identified by SwissProt entry names (for their accession numbers and gene names, see Table 1). Activities are given in enzyme classification numbers EC (green squares) and terms (blue squares). The various icons used in Figure 1 are shown below the graph at higher magnification. The left icon of the bottom line represents proteins named by their entry names within the figure. The middle icon indicates a publication, which is identified by the PMID number within the nearby white box. The PMID numbers identify those publications, which indicate that the respective protein contains an intrinsically disordered domain. The cell dish icon at the right side of the bottom indicates the origin of the cells. Within the figure, brown lines show the link of the protein to the origin cell lines MCF-7 (left side cell dish icon) and FTC-133 (right side cell dish icon). To see details, please zoom in.

### 2.2. Network Formation of Selected Proteins

Using Pathway Studio (version 12.3), we studied interactions of the 51 MCF-7 proteins and the 47 FTC-133 proteins indicated in Table 1 with emphasis on BCAR1 interactions which could lead to complex formation. We found that the proteins of each cell line formed a unique network, as indicated by the upper and the lower picture of Figure 2. Relating to direct interaction with the scaffolding potential of the identified proteins (Table 1), the role of BCAR1 in networks of mutual binding or direct regulation is shown in Figure 2 by gray lines, green arrows, and red lines.

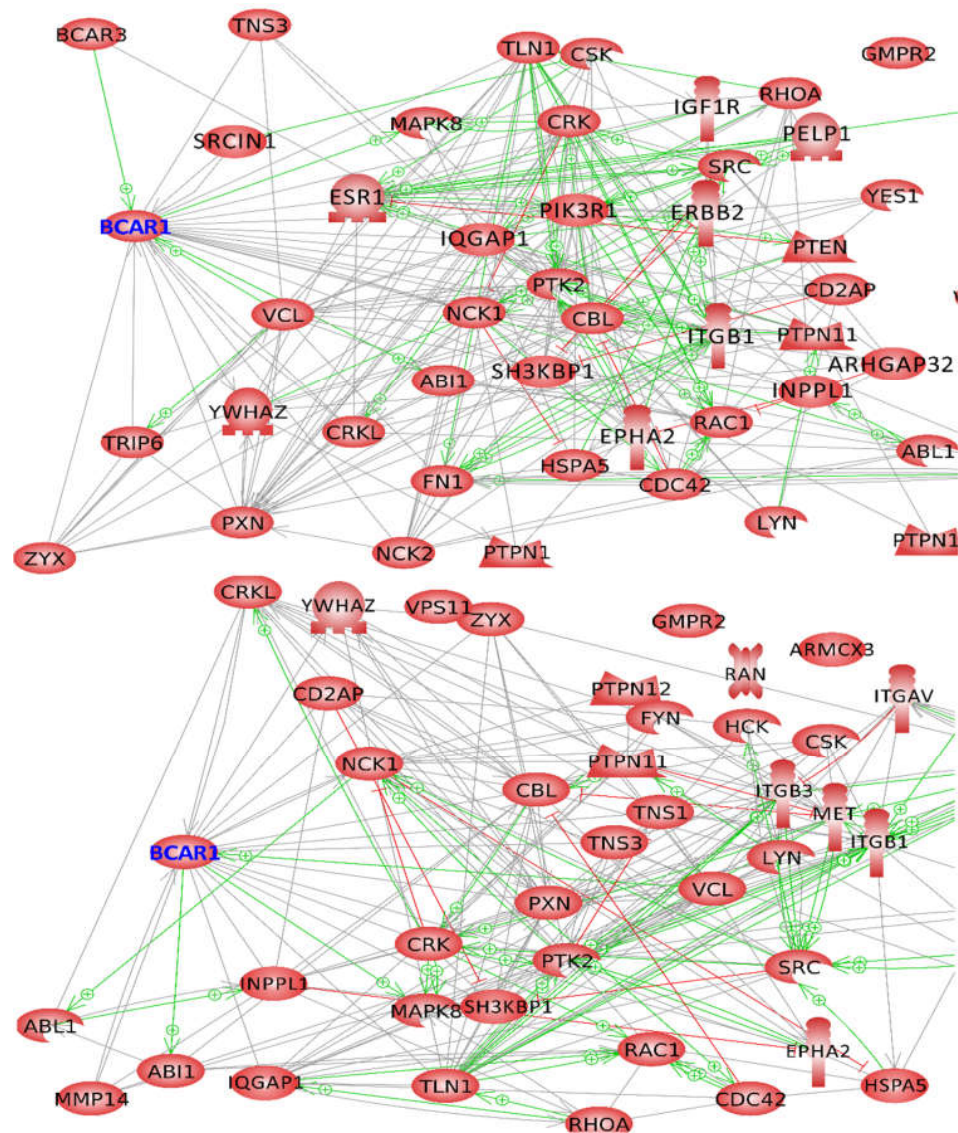


**Figure 2.** Interaction of the selected proteins obtained from proteome analysis of MCF-7 breast cancer cells (**upper picture**) and of FTC-133 thyroid cancer cells (**lower picture**). The icon labels refer to proteins by their human entry names (see also Table 1). The lines between the icons show various types of interaction. Gray lines indicate complex formation of the proteins connected with not exactly defined mutual influence. Green arrows point to complex formation with an activity enhancing effect on the protein at the arrowhead, red lines indicate complex formation with inhibition of the protein at the cross-piece. In both pictures, a gray connection between BCAR1 and CRK indicates complex formation, while a green arrow between VCL and BCAR1 with the head near BCAR1 indicates activation of BCAR1 by VCL and a green arrow between BCAR1 and MAPK8 with the head near MAPK8 indicates activation of MAPK8 by BCAR1. The interaction network was built using Pathway Studio v.12.3.

Both pictures of Figure 2 show that BCAR1 can bind proteins detected in the proteome analyses published in [35,36]. Of the proteins detected in the MCF7 [35] and also in the FTC-133 cells [36], CBL, CD2AP, CRK, CRKL, IQGAP1, NCK1, PTK2, PXN, SH3KBP1, SHIP2, TLN1, TNS3 and ZYX can interact with BCAR1 (full protein names are given in Table 1). Of further proteins capable of binding to BCAR1, we found ESR1, NCK2, PIK3R1 and SRCIN1 only in MCF-7 cells, while MMP14 and TNS1 were only detected in FTC-133 cells. Vinculin (VCL), which was found in both types of cells, triggers activation of BCAR1 by direct interaction, while ABI1, MAPK8 and BCAR3 detected only in MCF-7 cells are activated by BCAR1 (Figure 2, green arrows). Further regulatory effects on BCAR1 are exerted by TRIP6 and SRCIN1, which both were detected in MCF-7 cells only as well as by MMP14, which was only detected in FTC-133 cells. The 14-3-3 protein zeta/delta (YWHAZ), which was detected in both cell types, forms a complex with BCAR1 (Figure 2).

### 2.3. Influence of Selected Interaction on Cell Physiology

While using Pathway Studio, online mouse clicks on strings or arrows in the graphs of Figure 2 allowed us to retrieve literature about the protein interactions represented by lines and arrows linked to BCAR1.

#### 2.3.1. Proteins Binding to the Substrate Domain (SD) of BCAR1

In both cell types, the adapter molecule crk (CRK) and the Crk-like protein (CRKL) were detected in our proteome analyses published in refs. [35,36]. The quantitation scores calculated in the mentioned analyses for CRK and CRKL of MCF7 cells were  $12 \times 10^8$  and  $21 \times 10^8$ , those calculated for CRK and CRKL of FTC-133 cells were  $1.6 \times 10^8$  and  $2.9 \times 10^8$ . Interestingly, in FTC-133 cells, CRKL was visible under each incubation condition, while the concentration of FTC-133 CRK reached only detectable levels when the cells became confluent [36]. According to [5,21], these proteins bind to the BCAR1 substrate domain (SD) (Figure 3) after its YxxP motifs have been phosphorylated. If CRK is bound to BCAR1, formation of stress fibers is induced [44] and the activation of mitogen-activated protein kinase 8 (MAPK8) is favored [45]. Reversely, CRKL binding to BCAR1 impairs the connection of BCAR1 to the total focal adhesion complex (FA) [46], but promotes recruitment of procaspase-8, suppressing apoptosis and favoring cell migration [47]. If CRK is phosphorylated at its SH3 domain, CRK-BCAR1 dissociates and cell migration is prevented [48]. Zyxin (ZYG) competes with CRK for binding to BCAR1. Recruited from the cytoplasm, zyxin colocalizes with integrin and BCAR1. Upon mechanical stress, zyxin is involved in the re-organization of the cytoskeleton [49]. Similar effects on the regulation of the actin-cytoskeleton are exerted by TRIP6 (thyroid receptor interacting protein 6), another member of the zyxin family which only was detected in MCF-7 cells [50]. SHIP2 (SH2-containing inositol 5''- phosphatase 2) also binds to the phosphorylated SD of BCAR1 (Figure 3) [20]. Here, it becomes phosphorylated and activated for the de-phosphorylation of surrounding inositol, which favors cell adhesion [51]. Furthermore PIK3R1 (only detected in MCF-7 cells, see Table 1) associates with the proline-rich region of BCAR1, which leads to the reorganization of the cytoskeleton [52].

SH3 Homology Domain	Proline-rich Region	Substrate Domain (SD)	Serine-rich Domain	Substrate Binding Domain (SBD)	Focal Adhesion Targeting Domain
<ul style="list-style-type: none"> <li>• PTK2</li> <li>• PXN</li> <li>• VCL</li> <li>• TNS3</li> <li>• TLN</li> </ul>	<ul style="list-style-type: none"> <li>• PIK3R1</li> <li>• IQGAP1</li> </ul>	<ul style="list-style-type: none"> <li>• CRK, CRKL</li> <li>• NCK, NCK2</li> <li>• SHIP2</li> <li>• CBL</li> <li>• ZYX, TRIP6</li> </ul>	<ul style="list-style-type: none"> <li>• 14-3-3</li> </ul>	<ul style="list-style-type: none"> <li>• FYN</li> <li>• LYN</li> </ul>	<ul style="list-style-type: none"> <li>• PXN</li> </ul>

**Figure 3.** Proteins are indicated, which have been detected in our proteome analyses described in refs. [35,36]. They are assigned to BCAR1 domains and region described in the literature [see introduction, third section], with which they interact.

In addition, NCK1 and NCK2 bind to the SD domain of phosphorylated BCAR1 [53]. NCK mediates the interaction of BCAR1 with the GTPase-activating protein ARHGAP32



(only detected in MCF-7 cells). The complex of NCK-BCAR1-ARHGAP32 affects cell differentiation via CDC42 and RAC1 [54]. Another molecular complex containing BCAR1 and NCK is a critical link in signaling from the activated platelet-derived growth factor receptor beta (PDGF $\beta$ R) to the actin cytoskeleton [55]. NCK1 (commonly named NCK) and NCK2 regulate the actin cytoskeleton dynamic in slightly different ways [56]. The difference may be due to their different sensitivities to ubiquitination by the E3 ubiquitin-protein ligase CBL (CBL) [57]. CBL binds to membrane-associated BCAR1 via CRK or NCK [58]. Being a member of CBL-BCAR1-CRK (or NCK) complexes, CBL exerts several regulatory functions by mediating the ubiquitination and degradation of various proteins in a negative feedback manner [59]. Amongst those proteins are members of the src-family kinases [60,61], including lyn- and fyn-kinases (see Table 1), which are known to phosphorylate the SD domain of BCAR1 [62,63]. Associated with the SH3 domain-containing kinase-binding protein 1 (SH3KBP1 or CIN85), CBL forms another complex with BCAR1 [64]. This complex contributes to the regulation of cell adhesion and apoptosis [65]. If CBL and BCAR1 form complexes with ABL1, the complexes associate with C3G, BCAR/ABL and CRKL. Together, these proteins regulate cell adhesion and migration via paxillin (PXN) and focal adhesion kinase 1 (PTK2) [66]. Within this association, BCAR1 is highly tyrosine phosphorylated [67]. In addition, CBL binds to CD2AP [68], which connects the SH3 domain of BCAR1 with the actin cytoskeleton in a regulated manner [69].

Although the site where IQGAP1 associates with BCAR1 has not been exactly determined until now, it is known that its binding to the N-terminal region of BCAR1 needs phosphorylation of the tyrosines of BCAR1's SD, is stimulated by VEGF and plays a role in endothelial cell motility and angiogenesis [70]. Association of the matrix metalloproteinase-14 (MMP14) only detected in thyroid cells with BCAR1 at the edge of adhering cells has not been precisely localized. It is known, however, that it is initiated by phosphorylation of the substrate domain of BCAR1. After association, MMP14 is also phosphorylated [71].

### 2.3.2. Proteins Binding to other BCAR1 Domains

Besides the above-described proteins binding to the SD of BCAR1, there are proteins which bind to the N-terminal SH3 domain of BCAR1 (Figure 3) [5,20]. The mechanism of binding of different proteins under different conditions to this SH3 domain has been characterized by crystallographic analysis [20]. Focal adhesion kinase 1 (FAK1 or PTK2) binds to the SH3 domain of BCAR1, if it is pre-phosphorylated and BCAR1 phosphorylation occurs afterwards [72]. If tyrosines within the SH3 domain of BCAR1 are already phosphorylated, its interaction with FAK1 and recruitment of FAK1 to focal adhesions are inhibited [73]. If BCAR1 and FAK1 form a complex, tensin-3 co-localizes. This co-localization occurs in a focal adhesion complex depending on whether BCAR1 is phosphorylated or not [74]. Vinculin binds to the SH3 domain of BCAR1 together with FAK1 [27]. The BCAR1-FAK1-vinculin complex, which is found within focal adhesion complexes is required for stretch-induced phosphorylation of the BCAR1 SD. Furthermore, paxillin binds to the N-terminal regions, i.e., to the SH3 domain of BCAR1 via LD2/LD4 motifs [75]. In the latter case, paxillin forms complexes with talin which is phosphorylated subsequently before it can bind to BCAR1's SH3 domain [4,76].

According to references [5,21], the serine-rich region of BCAR1 is located at the c-terminal side of the BCAR1 substrate domain. If the underlying cell is attached to the extracellular matrix, YWHAZ binds to this serine-rich region [77]. An YWHAZ-BCAR1 complex appears to forward signals for actin polymerization. At the c-terminal side of the serine-rich domain, the carboxy-terminal domain is located. The interaction of SRC kinase signaling inhibitor 1 (SRCIN1 or p140Cap) with this BCAR1 domain triggers SRCIN1 phosphorylation and plays a role in controlling actin cytoskeleton organization in response to adhesive and growth factor signaling [78]. Moreover, paxillin can bind to the BCAR1's C-terminal region via its LD1 motif [75]. Bound to this site of BCAR1, paxillin anchors BCAR1 to the FA (Figure 3).

### 2.4. BCAR1, a Chain Link between Focal Adhesion and Cytoskeletal Proteins

Although BCAR1 emits various signals regulating cytoskeleton and cell adhesion, information about a direct binding of BCAR1 to actin and myosin proteins or to adhesion molecules such as cadherins or integrins was not found in literature. Therefore, we performed interaction analyses of MCF-7 (Figure 4, upper picture) and FTC-133 proteins (Figure 4, lower picture), examining the proteins which directly interact with BCAR1 as shown in Figure 2 together with the cytoskeletal proteins beta-actin, gamma-actin, myosin-9 and myosin-10 found in both cell types and with the adhesion proteins e-cadherin found in MCF-7 cells (Figure 4, upper picture) or the n-cadherin found in FTC-133 cells (Figure 4, lower picture). Figure 4 shows that in both types of cells, actins and myosins are linked to BCAR1 via TLN1 or IQGAP1 [79–83], while integrin beta 1 is associated with BCAR1 via PXN, VCL and IQGAP1 [84,85]. However, different cell–cell adhesion proteins were detected in the two cell types.

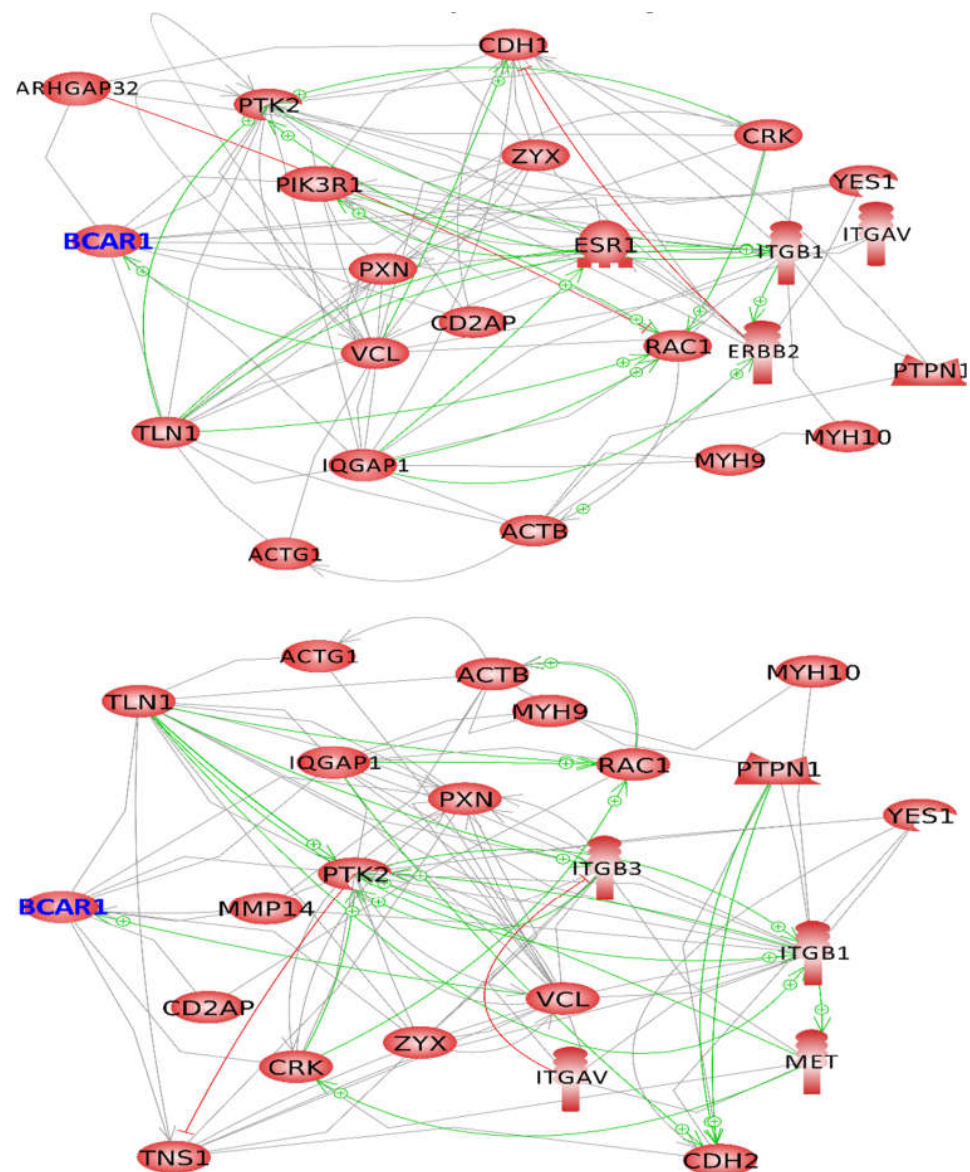


**Figure 4.** Selected proteins which form complexes with BCAR1, as indicated by gray lines. Of these proteins, TLN1 and IQGAP1 also form complexes with actins and myosins of MCF-7 breast cancer cells (**upper picture**) and of FTC-133 thyroid cancer cells (**lower picture**), establishing a link between the BCAR1 and the cytoskeleton. Regarding the cell–cell interaction proteins, CDH1 is connected to BCAR1 via PIK3R1 in MCF7 cells (**upper picture**), while CDH2 forms a complex with TNS1 and

BCAR1 in FTC-133 cells (**lower picture**). Additional links between BCAR1 and the growth factor receptors ESR1 (**upper picture**) and MET (**lower picture**) can be recognized. The icons indicate the proteins by their human entry names (see also Table 1). The lines between the icons show various types of interaction. Gray lines indicate complex formation of the proteins connected. Green arrows point to complex formation with an activity enhancing effect on the protein at the arrowhead, red lines indicate complex formation with inhibition of the protein at the cross-piece. The interaction network was built using Pathway Studio v.12.3.

CDH1 was found together with ARHGAP32, PIK3R1, ESR1 and ERBB2 only in MCF-7 cells, while CDH2 and ITGB3, MET, MMP14 and TNS1 were found only in FTC-133. Direct association of BCAR1 with ESR1 has a negative influence on breast cancer cell differentiation as it impairs mammary gland morphogenesis, if BCAR1 is over-expressed [86,87]. CDH1 interacts with BCAR1 indirectly via ARHGAP32 [88] or PIK3R1 [89], which both dock at BCAR1's SD. If PIK3R1 also binds to ERBB2 [90], the loss of CDH1 is induced [91]. In FTC-133 cells, CDH2, ITGB3 and MET are linked to BCAR1 via tensin-1 (TNS1). TNS1 binds to BCAR1 and is phosphorylated upon integrin activation [92]. In the absence of activated integrins, tensin is transferred to n-cadherin [93]. MMP14 binds to phosphorylated BCAR1 [71]. In confluent endothelial cell cultures, MMP14 is associated with integrin-beta1, while it is found jointly with  $\alpha v \beta 3$  integrins in migrating EC [94]. The association of the hepatocyte growth factor receptor (MET) with the CRK isoform CRK-II sends proliferative signals to the cells which harbor them [95]. Combined Figure 4 implies that there are links between BCAR1 and the cytoskeleton, between BCAR1 and adhesion proteins as well as between BCAR1 and growth factor receptors.

### 2.5. BCAR1's Belonging to Cellular Processes

To see which protein–protein interactions are included in which cellular processes, we looked at those cellular processes in which BCAR1 and at least another five selected proteins of the same cell type were included. We found a set of 18 identical processes, independently of whether we used the MCF-7 or the FTC-133 proteins (Figure 5). Seven of these processes were represented by equal proteins of both cell lines. In respect to the other 11 processes, different proteins of similar processes were reported. Because of the low coverage of these pathways by the selected proteins, an interpretation of these findings is difficult (Supplementary Table S1). However, it is remarkable that 17 of the pathways include FAK1, which catalyzes the linking of BCAR1 to the focal adhesion complexes initiating its SD phosphorylation [4,20,27,72–74]. Another 10 processes include BCAR1 and FAK1 together with CRK that uses phosphorylated SD of BCAR1 to form complexes with further proteins to send out different signals (Figure 6) [44,45,48–51].

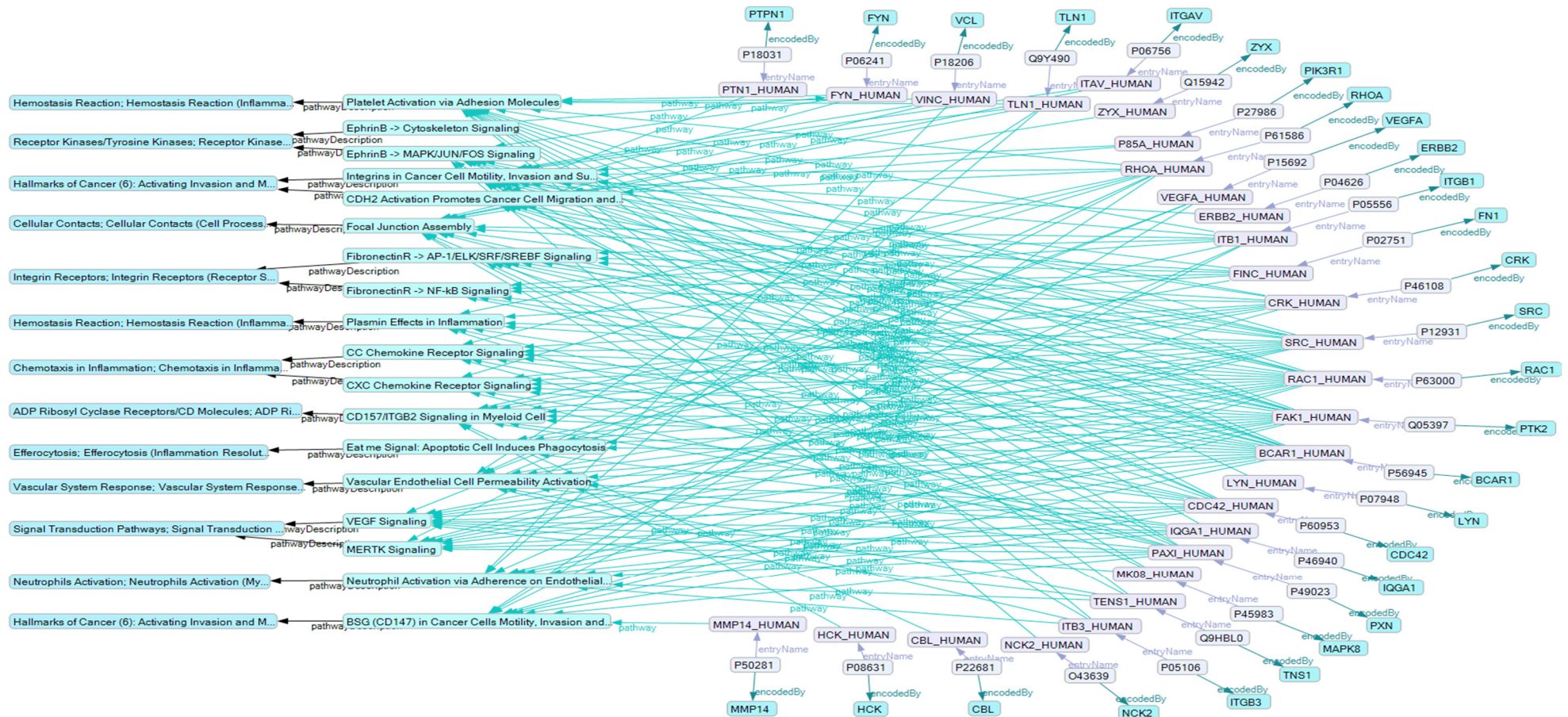


**Figure 5.** Overview on the participation of selected proteins in signaling pathways and processes. Proteins are identified by SwissProt accession numbers (AC#) and gene names shown at the right side of the figure. The arrows indicate participation of a protein in the pathway indicated within blue rectangles at the left side of the figure. The very left column shows the name of the group to which, according to Reactome, the pathways mentioned in the second column from left belong. (For further details, see Supplementary Table S1, or zoom in).

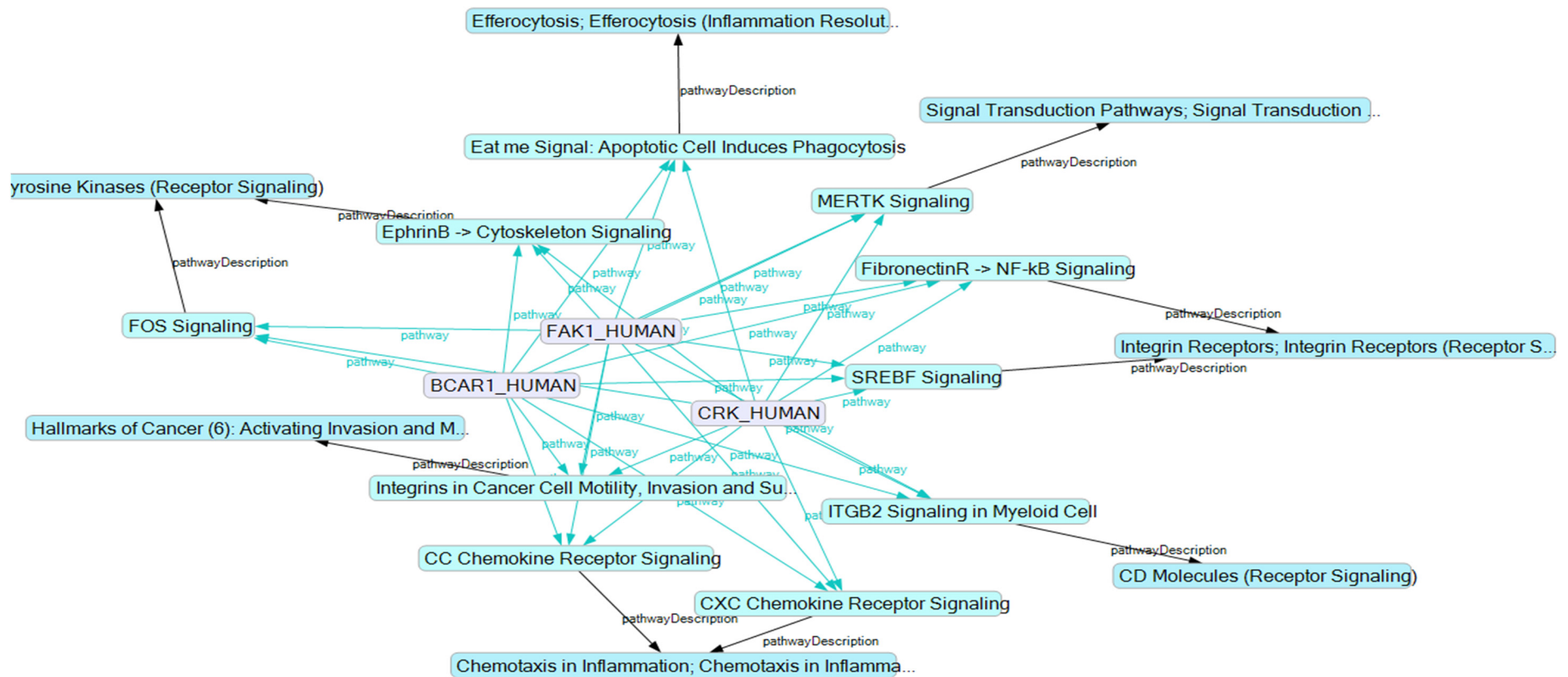


**Figure 6.** Signaling pathways, of which each includes BCAR1 and FAK1 (PTK2) and CRK. These pathways are included in Figure 5 but are shown here in more detail. The proteins are indicated by human entry names. The signaling pathways are named within light blue rectangles. They had been identified in Reactome assigned to their headings. Also see Supplementary Table S1.

### 3. Discussion

In this study, we applied functional network-based techniques to advance knowledge about possible targets, where the alteration of gravity force initiates changes of cellular behavior. Networks were established using data of earlier studies [35,36,84]. BCAR1 was selected as a central component of these networks because its activity is sensitive to forces that can change its three-dimensional conformation, enhancing or diminishing the accessibility for kinases [4,5]. As explained above, different accessibility for kinases changes the phosphorylation status of BCAR1, which subsequently scaffolds different proteins and exerts different effects on several signaling pathways.

The alteration of the phosphorylation of certain proteins under the condition of altered gravity has already been described. For example, an enhanced phosphorylation of profilin-1 was observed in confluent monolayers of FTC-133 cells, which did not form spheroids on an RPM but had accumulated fyn-kinase and caveolin 1 [36,96]. Endothelial cells cultured on a clinostat showed changes of phosphorylation of caveolin and nitric oxide synthetase [97,98]. Cultured on a Rotary Cell Culture System (RCCS), human mesenchymal stem cells reduced cofilin phosphorylation [99], while equal cells cultured on a three-dimensional clinostat intensified paxillin phosphorylation at their edges [100]. When macrophages are cultured on a two-dimensional clinostat, spleen tyrosine kinase (SYK) phosphorylation is reduced [101]. Simulated microgravity influences the phosphorylation level of phosphoinositide 3-kinase (PI3K) in OSE-3T3 cells [102]. In vivo, a hindlimb suspension of mice decreased the phosphorylation of ribosomal protein S6 kinase 1 [103]. Therefore, this semantic study challenges an experimental search for a direct link between the lack of gravity force to pull cells constantly towards the center of the Earth and the phosphorylation of BCAR1.

It has been shown that a cell line includes 10,000 to 12,000 different proteins [104]. As such, one can assume that in the proteome analyses, evaluated proteins represent about 50% to 70% of potentially present ones [35,36]. Despite the shortcomings, our proteome analyses unveiled various proteins interacting with BCAR1. BCAR1 consists of five domains, of which the substrate domain (SD) is the most force-sensitive one [4,5]. Comparing studies of microgravity research with literature about protein complexes which dock at BCAR1's SD, we noticed common physiological effects. For example, CRK interacts with BCAR1 via the force-sensitive SD domain. This type of complex formation induces the formation of stress fibers and the activation of MAPK8 [44,45,48]. The altered formation of stress fibers and activation of MAPK8 were also observed in cells exposed to simulated microgravity [105–108]. Furthermore, within a focal adhesion complex, BCAR1 and CRK together may associate with TRIP6 detected in MCF-7 cells [35,48,109]. Scaffolded by BCAR1 and CRK TRIP6 interacts with NF- $\kappa$ B (nuclear factor  $\kappa$ B) linking cell adhesion and nuclear transcription [110]. This fits to our recent experimental work, which showed that altered gravity has a remarkable influence on the cellular localization of NF- $\kappa$ B in MCF-7 cells [111].

CBL is a further protein that interacts with BCAR1 via the SD-bound CRK [58] and had attracted attention in microgravity research. Associated with BCAR1 and CRK, CBL catalyzes the link of ubiquitin to several different target proteins, initiating their degradation [59–61]. Linking ubiquitin or ubiquitin-like molecules to the  $\epsilon$ -amino group of lysine residues in target proteins regulates many cellular processes [112,113]. They lead to the degradation of distinct proteins but also to the stabilization of others. This type of post-translational modification was observed on many proteins, which are upregulated in spheroids formed during cell incubation on an RPM as compared to control cells [3]. Among the proteins of which the degradation is mediated by CBL are fyn- and lyn- kinases, which are the main kinases phosphorylating the SD of BCAR1 [61]. Consequently, studies of interest are those showing that L6 myoblasts enhanced the expression of muscle-atrophy-associated CBL during clinorotation [114] and that activation of CBL in microgravity induced muscle atrophy [115].

Moreover, the inositol metabolism plays a role in the adjustment of animal and plant cells to microgravity [116,117]. In both, the MCF-7 and FTC-133 cell lines SHIP2 (also named INPPL1) was found, which is activated after binding to the phosphorylated SD of BCAR1 [20,51]. This enzyme de-phosphorylates phosphatidylinositol-3,4,5-trisphosphate (PtdIns(3,4,5)P<sub>3</sub>) to PtdIns(3,4)P<sub>2</sub>, downregulating PI3K (phosphoinositide 3-kinase) pathways. PIK3R1 was detected in MCF-7 cells. When it forms complexes with BCAR1, it activates signaling pathways which lead to the re-organization of the cytoskeleton [52,118]. The hindlimb unloading of rats downregulates the PI3K/pAkt pathway inducing muscle atrophy [119], and the inhibition of PI3K (or NFκB) prevents the spheroid formation of breast cancer cells in ultra-low attachment plates [120]. The latter observation is supported by our recent proteome analysis, which unveiled 40% more PIK3R1 proteins in MCF-7 spheroids than in MCF-7 adherent cells [35]. In addition, CRKL interacts with BCAR1 via the force-sensitive SD domain. CRKL-BCAR1 complexes impair FA-mediated binding, while they suppress apoptosis by procaspase-8 inactivation [47,48]. This could explain that cells survive a detachment from the bottom of a culture flask during the formation of spheroids. The hypothesis is supported by the observation that procaspase-8 is inactivated when breast cancer cells detach from their natural substratum and fill breast ducts without suffering anoikis [121].

Via complex formation, the SD of BCAR1 influences various small GTPases [54,71]. In recent years, a number of studies have been published, which show that microgravity-induced changes of small GTPase activity play a role in the adjustment of various cells to altered gravity [122], e.g., of endothelial cells [123], glioma cells [124], stem cells [125] and cancer cells [126]. The changes of small GTPase activities accompany alterations of adhesion, migration and cytoskeletal rearrangements [124,126–128] as well as cell differentiation and morphogenesis [125,129].

Several cell functions and pathways were identified in which BCAR1, FAK1 and CRK are involved together (Supplementary Table S1). They include apoptosis, integrin function, cytoskeleton signaling, chemokine signaling and cancer cell motility (Figure 6). All these functions were observed when adaptation of cells to altered gravity was studied. Information about such studies can be retrieved in relevant databases. A few recent publications are given by refs. [130–134].

The comprehensive information collected using linked open data resources and our experiments suggests that changes in force-dependent phosphorylation or the de-phosphorylation of SD, the most force-sensitive part of BCAR1, cause similar changes in cellular behavior as when exposing cells to an RPM or a spaceflight. Though this suggestion is based on many studies, an influence of the alteration of gravity on the phosphorylation status of the SD of BCAR1 still needs verification by further experiments. However, even though a microgravity-dependent phosphorylation of SD will be proven, the question remains whether this change is caused by forces of motor proteins [135,136] linked to cellular adhesion or by a failure of gravity force pulling cells constantly to the center of the Earth. Figure 4 shows that there are at least indirect links between BCAR1 and myosins X or IX via proteins such as talin, IQGAP1 or between BCAR1 and integrins via focal adhesion kinase, paxillin and vinculin. Such links could also be the source of the force affecting BCAR1. Still, an influence of annulling gravity forces on the intrinsically disordered domain of BCAR1 appears possible, since size determinations of tissue cancer cells indicated volumes varying between 1000 and 2000 fL [137]. Assuming a density of around 1.05 kg/L, a cancer cell weighs between 1 and 2 ng. Hence, gravity force acting on one whole cell could be around 15 pN as long as a culture flask stays stationary in an incubator under normal 1 g condition. If this force of constantly pulling a cell towards the center of the Earth is totally or partially annulled by any technique [96,138,139], cells behave as if the force-dependent phosphorylation of BCAR1 had changed. This appears explainable, as the gravity force affecting a whole cell is higher than the force needed to stretch an intrinsically disordered domain of a protein [25,140].

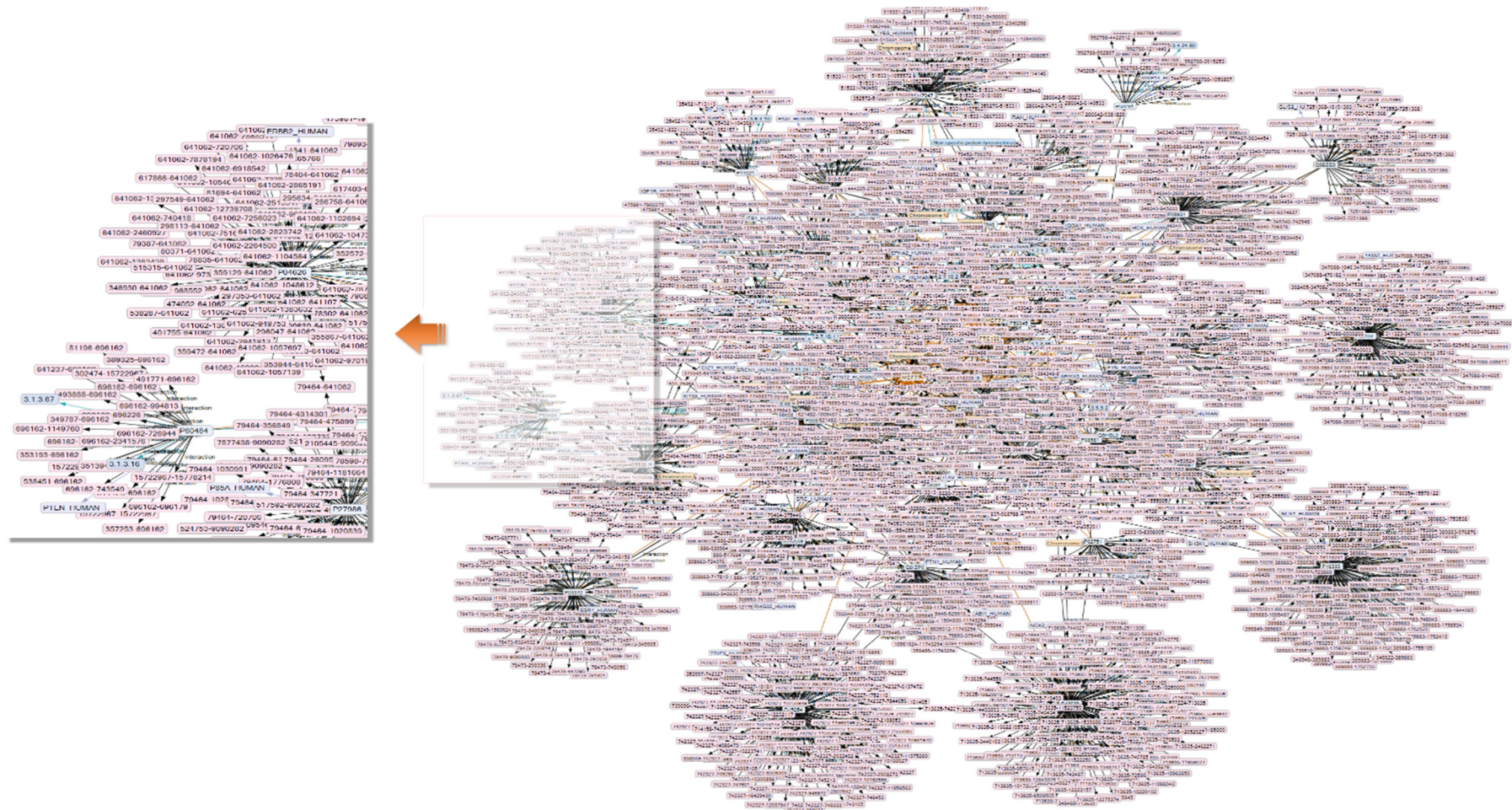


**Figure 7.** Two-level interactome. The first level is indicated by black nodes containing light blue rectangles with SwissProt accession numbers. Orange lines show the cell line origin of the proteins. The connection of the nodes with black lines corresponds to the networks shown in Figure 2. The second level is indicated by pink rectangles showing IntAct interaction numbers. The insert shows a magnification of the indicated part of the overview with legible numbers. The whole picture can be viewed for details at high magnification in Supplementary Figure S1. To see details here, please zoom in.



In addition, a change of BCAR1 activity is not limited to effects on or from the proteins forming the networks of Figure 2. Even if only a second level of interaction is considered, the complexity of the network enhances up to more than 1300 participants. The two-level interaction network shown in Figure 7 indicates that each of the proteins named in Table 1 (black spots with SwissProt AC# in white squares) interacts with further proteins (pink squares with IntAct interaction numbers). Despite the complexity, the KE allows one to contextualize all participants and interactions for understanding details of the system (see also Supplementary Figure S1). Graphical queries account for the close investigation of each and every sub-network to verify dependencies in more detail. This provides preconditions to further investigate the influence of additional parameters. One of them is the time of exposure to microgravity, which urgently needs to also be studied in the BCAR1 system, as it has been done for other proteins [141].

## 4. Materials and Methods

### 4.1. Proteome Data

Proteins were obtained by mass spectrometry from MCF-7 human breast adenocarcinoma cells and from FTC-133 human follicular thyroid carcinoma cells according to protocols described in [35,36]. Prior to analysis, both types of cells had been grown either within a monolayer under normal 1 g laboratory conditions or exposed to an RPM, where one part remained adherent (AD cells), while the other one formed three-dimensional aggregates (MCS cells). Monolayer cells cultured under 1 g, AD cells, and MCS cells were harvested and pelleted in separate samples. Each sample was subjected to a proteome analysis. In total, 12 different cell samples, i.e., four per incubation condition, were analyzed to determine as many proteins as possible of MCF-7 cells, and five pellets were investigated to identify proteins of FTC-133 cells.

Mass spectrometry was performed, as described in detail earlier [35,36]. Briefly, cells were lysed. Their proteins were digested overnight at 37 °C with endoproteinase Lys-C (Wako Chemicals GmbH, Neuss, Germany). The digested peptides were purified and then separated using the Thermo easy n-LC 1000 system (Thermo Scientific, Waltham, MA, USA). The peptides eluting from the column were directly sprayed into a Q Exactive HF mass spectrometer (Thermo Scientific, Waltham, MA, USA) via a nano-electrospray ionization source (Thermo Scientific, Waltham, MA, USA) [142,143]. The mass spectrometer was operated in a data-dependent top 15 mode. Survey scans and fragmentation scans were acquired at resolutions of 60,000 and 15,000, respectively ( $m/z = 200$ ). Fragmentation was performed on precursors isolated within a window of 1.4  $m/z$  with a normalized collision energy setting of 27.

Raw data from the mass spectrometer were processed using MaxQuant computational proteomics platform version 1.5.2.22 (Computational Systems Biochemistry, Max-Planck-Gesellschaft, Munich, Germany) [144] using the standard parameters. At least 5900 different proteins were identified in five FTC-133 cell samples [36], and 6500 different proteins were found in 12 MCF-7 cell samples [35]. These proteins formed the base for applying the MaxLfq algorithm to determine the relative protein concentration by delayed normalization, as explained by Cox et al. in detail [145]. This label-free quantification technology is based on the assumption that a majority of proteins exists which does not change between the samples of a cell line.

### 4.2. Searching Proteins Interacting with BCAR1

To search proteins co-mentioned with BCAR1 in literature, we used the STRING v11.0 tool [146] (available at <https://string-db.org/>, accessed on 21 July 2021) and in addition searched dbPTM [147] (available at <http://dbptm.mbc.nctu.edu.tw>, accessed on 1 November 2020). Direct interaction between the selected proteins was determined using Pathway Studio v.12.3 software (<https://www.pathwaystudio.com/>, accessed on 21 July 2021; Elsevier Research Solutions, Amsterdam, the Netherlands). After entering relevant UniProt accession numbers, this software enables collecting information from a full text

of articles about the interaction of proteins. Literature indicating interactions is unveiled online by mouse clicks on strings or arrows connecting icons.

#### 4.3. Creation of a Semantic Network

To create a semantic network, harmonize the content from multiple resources, and allow for graphical querying and reasoning, experimental data were imported to establish an initial resource description framework (RDF) knowledge base using KE (Melissa Informatics, Rancho Santa Margarita, CA, USA—former IO Informatics). This tool allows one to create, merge, and/or align semantic knowledge bases (SKB) in the form of RDF serializations as files or in backend databases and to configure and connect them to public semantic protocol and RDF query language (SPARQL) endpoints for query and imports [37,148]. Its import functions provide abilities for nomenclature alignment, to set or automate reification IDs for blank nodes, and to establish mapping for spreadsheets or XML alignment [149,150]. After importing the experimental proteomics data, an initial partial ontology imported from UniProt (<https://www.uniprot.org>, accessed on 21 July 2021; versions 2020-06 and 2021-01) XML-RDF format was transformed into a core RDF representation. A thesaurus manager was used to harmonize synonyms and avoid duplication during the import process.

The UniProt content was queried for each of the proteins using its SPARQL endpoint. This added functional, interaction and complex formation properties to augment the information on the enzymes and reported protein functions [149]. The information collected was used to retrieve content from the NCBI Entré resources OMIM, PubMed, and Biosystems by means of graphical queries and to import their results using the NCBI Connector API [151]. Parts of KEGG (Kyoto Encyclopedia of Genes and Genoms) and Reactome (<https://reactome.org/PathwayBrowser/>, accessed on 21 July 2021; v.75, Release 7 December 2020) [152] were used to validate pathway information. Protein–protein interactions were retrieved in IntAct (<https://ebi.ac.uk/intact/>, accessed on January 2021) and MINT (<https://mint.bio.uniroma2.it/>, accessed on 21 July 2021) databases.

## 5. Conclusions

From the network analysis presented, we conclude that the application of semantic tools such as KE and Pathway Studio, which help to look at a specific subgroup of thousands of proteins usually unveiled by proteome analyses of whole cells, will be useful to extract functional information from proteome analyses and better support one's understanding of complex cellular processes. Using this exemplary application of the method, we conclude that BCAR1 could be a primary target of Earth's gravity. Experiments on changes of the phosphorylation of BCAR1 under microgravity now appear to be a promising way to explore how gravity affects human tissue cells. In this context, we can also look at the influence of the time of exposure on the quantities of phosphorylated and un-phosphorylated BCAR1 molecules.

**Supplementary Materials:** The following are available online at <https://www.mdpi.com/article/10.3390/computation9080081/s1>, Supplementary Table S1: List of pathways and processes, which include BCAR1 and at least another five proteins of Table 1. Details are given about coverage and participating proteins of both cell lines. Supplementary Figure S1: Two-level protein interaction network: Violet arrow icons and their violet relationship lines indicate interactions. Numbers indicate IntAct designation of interaction. Interaction participants are not shown to simplify the graph. Proteins are identified with their icons labeled with UniProt accession numbers. Orange lines indicate the originating cancer cell line.

**Author Contributions:** E.G., J.B., conceptualization; D.G., cell culturing; E.G., J.B., H.S., software and data evaluation; J.H., J.B., validation; E.G., J.B. writing—original draft preparation; E.G., J.H., J.B., writing—review and editing; D.G., funding acquisition. All authors have read and agreed to the published version of the manuscript.

**Funding:** This research was funded by Deutsches Zentrum für Luft-und Raumfahrt (DLR), BMWi projects 50WB1524 and 50WB1924 (D.G.)

**Data Availability Statement:** Not applicable.

**Acknowledgments:** We thank Nagarjuna Nagaraj of the biochemistry core facility at the Max-Planck Institute of Biochemistry for performing proteomic sample preparation and measurements; the Deutsche Luft-und Raumfahrt Gesellschaft for supporting the purchase of the Pathway Studio license and Melissa Informatics for granting a Knowledge Explorer license.

**Conflicts of Interest:** The authors declare no competing interests.

## Abbreviations

LOD	linked open data;
SKB	semantic knowledgebase;
KE	knowledge explorer;
RDF	resource description framework;
SPARQL	semantic protocol and RDF query language;
RPM	random positioning machine;
FA	focal adhesion complex;
AD	adherent cells;
3D	three dimensional;
CM	consensus motif;
PK	protein kinase,
PP	protein phosphatase,
RCCS	Rotary Cell Culture System,
ROS	reactive oxygen species;
pN	piconewton;
SD	substrate domain;
Cas	CRK-associated substrate;
BCAR1	breast cancer anti-estrogen resistance protein 1;
SwissProt AC#	SwissPro accession number.

## References

1. Strauch, S.; Grimm, D.; Corydon, T.J.; Krüger, M.; Bauer, J.; Lebert, M.; Wise, P.; Infanger, M.; Richter, P. Current knowledge about the impact of microgravity on the proteome. *Expert Rev. Proteom.* **2019**, *16*, 5–16. [[CrossRef](#)]
2. Warnke, E.; Pietsch, J.; Kopp, S.; Bauer, J.; Sahana, J.; Wehland, M.; Krüger, M.; Hemmersbach, R.; Infanger, M.; Lützenberg, R.; et al. Cytokine Release and Focal Adhesion Proteins in Normal Thyroid Cells Cultured on the Random Positioning Machine. *Cell. Physiol. Biochem.* **2017**, *43*, 257–270. [[CrossRef](#)]
3. Bauer, J.; Wehland, M.; Infanger, M.; Grimm, D.; Gombocz, E. Semantic Analysis of Posttranslational Modification of Proteins Accumulated in Thyroid Cancer Cells Exposed to Simulated Microgravity. *Int. J. Mol. Sci.* **2018**, *19*, 2257. [[CrossRef](#)] [[PubMed](#)]
4. Sawada, Y.; Tamada, M.; Dubin-Thaler, B.J.; Cherniavskaya, O.; Sakai, R.; Tanaka, S.; Sheetz, M.P. Force sensing by mechanical extension of the Src family kinase substrate p130Cas. *Cell* **2006**, *127*, 1015–1026. [[CrossRef](#)]
5. Goldmann, W.H. Vinculin-p130 Cas interaction is critical for focal adhesion dynamics and mechano-transduction. *Cell Biol. Int.* **2013**, *38*, 283–286. [[CrossRef](#)] [[PubMed](#)]
6. Karabulut, N.P.; Frishman, D. Sequence- and Structure-Based Analysis of Tissue-Specific Phosphorylation Sites. *PLoS ONE* **2016**, *11*, e0157896. [[CrossRef](#)]
7. Hunter, T. Protein kinases and phosphatases: The Yin and Yang of protein phosphorylation and signaling. *Cell* **1995**, *80*, 225–236. [[CrossRef](#)]
8. Vandermarliere, E.; Martens, L. Protein structure as a means to triage proposed PTM sites. *Proteomics* **2013**, *13*, 1028–1035. [[CrossRef](#)] [[PubMed](#)]
9. De Oliveira, P.S.L.; Ferraz, F.A.N.; Pena, D.A.; Pramio, D.T.; Morais, F.A.; Schechtman, D. Revisiting protein kinase–substrate interactions: Toward therapeutic development. *Sci. Signal.* **2016**, *9*, re3. [[CrossRef](#)] [[PubMed](#)]
10. Karasev, D.A.; Veselova, D.A.; Veselovsky, A.V.; Sobolev, B.N.; Zgodina, V.G.; Archakov, A.I. Spatial features of proteins related to their phosphorylation and associated structural changes. *Proteins Struct. Funct. Bioinform.* **2017**, *86*, 13–20. [[CrossRef](#)]
11. Uppala, J.K.; Ghosh, C.; Sathe, L.; Dey, M. Phosphorylation of translation initiation factor eIF 2 $\alpha$  at Ser51 depends on site- and context-specific information. *FEBS Lett.* **2018**, *592*, 3116–3125. [[CrossRef](#)]

12. Ithychanda, S.S.; Fang, X.; Mohan, M.L.; Zhu, L.; Tirupula, K.C.; Naga Prasad, S.; Wang, Y.X.; Karnik, S.S.; Qin, J. A mechanism of global shape dependent recognition and phosphorylation of filamin by protein kinase A. *J. Biol. Chem.* **2015**, *290*, 8527–8538. [[CrossRef](#)]
13. Su, M.-G.; Weng, J.T.-Y.; Hsu, J.B.-K.; Huang, K.-Y.; Chi, Y.-H.; Lee, T.-Y. Investigation and identification of functional post-translational modification sites associated with drug binding and protein-protein interactions. *BMC Syst. Biol.* **2017**, *11*, 69–80. [[CrossRef](#)]
14. Pelaseyed, T.; Viswanatha, R.; Sauvanet, C.; Filter, J.J.; Goldberg, M.L.; Bretscher, A. Ezrin activation by LOK phosphorylation involves a PIP2-dependent wedge mechanism. *eLife* **2017**, *6*, 22759. [[CrossRef](#)]
15. Acebrón, I.; Righetto, R.D.; Schoenherr, C.; De Buhr, S.; Redondo, P.; Culley, J.; Rodríguez, C.F.; Daday, C.; Biyani, N.; Llorca, O.; et al. Structural basis of Focal Adhesion Kinase activation on lipid membranes. *EMBO J.* **2020**, *39*, 104743. [[CrossRef](#)] [[PubMed](#)]
16. Travers, T.; Shao, H.; Joughin, B.A.; Lauffenburger, D.A.; Wells, A.; Camacho, C.J. Tandem phosphorylation within an intrinsically disordered region regulates ACTN4 function. *Sci. Signal.* **2015**, *8*, ra51. [[CrossRef](#)] [[PubMed](#)]
17. Snyder, J.L.; McBeath, E.; Thomas, T.N.; Chiu, Y.J.; Clark, R.L.; Fujiwara, K. Mechanotransduction properties of the cytoplasmic tail of PECAM-1. *Biol. Cell* **2017**, *109*, 312–321. [[CrossRef](#)] [[PubMed](#)]
18. Röper, J.C.; Mitrossilis, D.; Stirnemann, G.; Waharte, F.; Brito, I.; Fernandez-Sanchez, M.E.; Baaden, M.; Salamero, J.; Farge, E. The major  $\beta$ -catenin/E-cadherin junctional binding site is a primary molecular mechano-transducer of differentiation in vivo. *eLife* **2018**, *7*, e33381. [[CrossRef](#)] [[PubMed](#)]
19. Defilippi, P.; Di Stefano, P.; Cabodi, S. p130Cas: A versatile scaffold in signaling networks. *Trends Cell Biol.* **2006**, *16*, 257–263. [[CrossRef](#)] [[PubMed](#)]
20. Wisniewska, M.; Bossenmaier, B.; Georges, G.; Hesse, F.; Dangl, M.; Künkele, K.-P.; Ioannidis, I.; Huber, R.; Engh, R.A. The 1.1Å Resolution Crystal Structure of the p130cas SH3 Domain and Ramifications for Ligand Selectivity. *J. Mol. Biol.* **2005**, *347*, 1005–1014. [[CrossRef](#)]
21. Mace, P.D.; Wallez, Y.; Dobaczewska, M.K.; Lee, J.J.; Robinson, H.; Pasquale, E.B.; Riedl, S.J. NSP-Cas protein structures reveal a promiscuous interaction module in cell signaling. *Nat. Struct. Mol. Biol.* **2011**, *18*, 1381–1387. [[CrossRef](#)]
22. Hotta, K.; Ranganathan, S.; Liu, R.; Wu, F.; Machiyama, H.; Gao, R.; Hirata, H.; Soni, N.; Ohe, T.; Hogue, C.; et al. Biophysical Properties of Intrinsically Disordered p130Cas Substrate Domain—Implication in Mechanosensing. *PLoS Comput. Biol.* **2014**, *10*, e1003532. [[CrossRef](#)] [[PubMed](#)]
23. Lu, C.; Wu, F.; Qiu, W.; Liu, R. P130Cas substrate domain is intrinsically disordered as characterized by single-molecule force measurements. *Biophys. Chem.* **2013**, *180–181*, 37–43. [[CrossRef](#)] [[PubMed](#)]
24. Liu, W.; Liu, X.; Zhu, G.; Lu, L.; Yang, D. A method for determining structure ensemble of large disordered protein: Application to a mechanosensing protein. *J. Am. Chem. Soc.* **2018**, *140*, 11276–11285. [[CrossRef](#)] [[PubMed](#)]
25. Schiller, H.B.; Fässler, R. Mechanosensitivity and compositional dynamics of cell-matrix adhesions. *EMBO Rep.* **2013**, *14*, 509–519. [[CrossRef](#)] [[PubMed](#)]
26. Donato, D.M.; Ryzhova, L.M.; Meenderink, L.M.; Kaverina, I.; Hanks, S.K. Dynamics and Mechanism of p130Cas Localization to Focal Adhesions. *J. Biol. Chem.* **2010**, *285*, 20769–20779. [[CrossRef](#)]
27. Janostiak, R.; Brábek, J.; Auernheimer, V.; Tatarova, Z.; Lautscham, L.A.; Dey, T.; Gemperle, J.; Merkel, R.; Goldmann, W.H.; Fabry, B.; et al. CAS directly interacts with vinculin to control mechanosensing and focal adhesion dynamics. *Cell. Mol. Life Sci.* **2013**, *71*, 727–744. [[CrossRef](#)]
28. Geiger, B.; Berdshadsky, A. Exploring the neighborhood: Adhesion-coupled cell mechanosensors. *Cell* **2002**, *110*, 139–142. [[CrossRef](#)]
29. Barrett, A.; Pellet-Many, C.; Zachary, I.C.; Evans, I.M.; Frankel, P. p130Cas: A key signalling node in health and disease. *Cell. Signal.* **2013**, *25*, 766–777. [[CrossRef](#)]
30. Cabodi, S.; Camacho-Leal, M.D.P.; Di Stefano, P.; Defilippi, P. Integrin signalling adaptors: Not only figurants in the cancer story. *Nat. Rev. Cancer* **2010**, *10*, 858–870. [[CrossRef](#)]
31. Ratushnyy, A.Y.; Buravkova, L.B. Expression of focal adhesion genes in mesenchymal stem cells under simulated microgravity. *Dokl. Biochem. Biophys.* **2017**, *477*, 354–356.
32. Tang, H.; Hao, Q.; Fitzgerald, T.; Sasaki, T.; Landon, E.J.; Inagami, T. Pyk2/CAK Tyrosine Kinase Activity-mediated Angiogenesis of Pulmonary Vascular Endothelial Cells. *J. Biol. Chem.* **2002**, *277*, 5441–5447. [[CrossRef](#)] [[PubMed](#)]
33. Nassef, M.; Melnik, D.; Kopp, S.; Sahana, J.; Infanger, M.; Lützenberg, R.; Relja, B.; Wehland, M.; Grimm, D.; Krüger, M. Breast Cancer Cells in Microgravity: New Aspects for Cancer Research. *Int. J. Mol. Sci.* **2020**, *21*, 7345. [[CrossRef](#)]
34. Konstantinovskiy, S.; Davidson, B.; Reich, R. Ezrin and BCAR1/p130Cas mediate breast cancer growth as 3-D spheroids. *Clin. Exp. Metastasis* **2012**, *29*, 527–540. [[CrossRef](#)] [[PubMed](#)]
35. Sahana, J.; Nassef, M.Z.; Wehland, M.; Kopp, S.; Krüger, M.; Corydon, T.J.; Infanger, M.; Bauer, J.; Grimm, D. Decreased E-Cadherin in MCF7 Human Breast Cancer Cells Forming Multicellular Spheroids Exposed to Simulated Microgravity. *Proteomics* **2018**, *18*, e1800015. [[CrossRef](#)]
36. Bauer, J.; Kopp, S.; Schlagberger, E.M.; Grosse, J.; Sahana, J.; Riwaldt, S.; Wehland, M.; Luetzenberg, R.; Infanger, M.; Grimm, D. Proteome Analysis of Human Follicular Thyroid Cancer Cells Exposed to the Random Positioning Machine. *Int. J. Mol. Sci.* **2017**, *18*, 546. [[CrossRef](#)]

37. Gombocz, E.A.; Stanley, R.A.; Rockey, C.; Nishimura, T. Data Integration Framework for Discovery and Validation: Smart Merging of Experimental and Public Data Across Ontologies and Taxonomies. In Proceedings of the 2018 BIO-IT World conference, Boston, MA, USA, 16–18 April 2018. Available online: <https://de.slideshare.net/crockey/data-integration-framework-for-discovery-and-validation> (accessed on 1 March 2020).
38. Soule, H.D.; Vazquez, J.; Long, A.; Albert, S.; Brennan, M. A Human Cell Line from a Pleural Effusion Derived from a Breast Carcinoma. *J. Natl. Cancer Inst.* **1973**, *51*, 1409–1416. [[CrossRef](#)]
39. Kang, H.; Rho, J.G.; Kim, C.; Tak, H.; Lee, H.; Ji, E.; Ahn, S.; Shin, A.-R.; Cho, H.-I.; Huh, Y.H.; et al. The miR-24-3p/p130Cas: A novel axis regulating the migration and invasion of cancer cells. *Sci. Rep.* **2017**, *7*, 44847. [[CrossRef](#)]
40. Goretzki, P.E.; Frilling, A.; Simon, D.; Roeher, H.-D. Growth Regulation of Normal Thyroids and Thyroid Tumors in Man. *Methods Mol. Biol.* **1990**, *118*, 48–63. [[CrossRef](#)]
41. Simon, D.; Goretzki, P.E.; Gorelev, V.; Ebling, B.; Reishaus, E.; Lyons, J.; Haubruck, H.; Röher, H.D. Significance of P53 in human thyroid tumors. *World J. Surg* **1994**, *18*, 535–541. [[CrossRef](#)]
42. Pietsch, J.; Sickmann, A.; Weber, G.; Bauer, J.; Egli, M.; Wildgruber, R.; Infanger, M.; Grimm, D. A proteomic approach to analysing spheroid formation of two human thyroid cell lines cultured on a random positioning machine. *Proteomics* **2011**, *11*, 2095–2104. [[CrossRef](#)] [[PubMed](#)]
43. Ma, X.; Pietsch, J.; Wehland, M.; Schulz, H.; Saar, K.; Hübner, N.; Bauer, J.; Braun, M.; Schwarzwälder, A.; Segerer, J.; et al. Differential gene expression profile and altered cytokine secretion of thyroid cancer cells in space. *FASEB J.* **2014**, *28*, 813–835. [[CrossRef](#)] [[PubMed](#)]
44. Murakami, H.; Iwashita, T.; Asai, N.; Iwata, Y.; Narumiya, S.; Takahashi, M. Rho-dependent and independent tyrosine phosphorylation of focal adhesion kinase, paxillin and p130Cas mediated by Ret kinase. *Oncogene* **1999**, *18*, 1975–1982. [[CrossRef](#)]
45. Kodama, H.; Fukuda, K.; Takahashi, E.; Tahara, S.; Tomita, Y.; Ieda, M.; Kimura, K.; Owada, K.M.; Vuori, K.; Ogawa, S. Selective Involvement of p130Cas/Crk/Pyk2/c-Src in Endothelin-1-Induced JNK Activation. *Hypertension* **2003**, *41*, 1372–1379. [[CrossRef](#)]
46. Salgia, R.; Pisick, E.; Sattler, M.; Li, J.-L.; Uemura, N.; Wong, W.-K.; Burky, S.A.; Hirai, H.; Chen, L.B.; Griffin, J.D. p130CAS Forms a Signaling Complex with the Adapter Protein CRKL in Hematopoietic Cells Transformed by the BCR/ABL Oncogene. *J. Biol. Chem.* **1996**, *271*, 25198–25203. [[CrossRef](#)]
47. Graf, R.; Barbero, S.; Keller, N.; Chen, L.; Uryu, S.; Schlaepfer, D.; Stupak, D. Src-inducible association of CrkL with pro-caspase-8 promotes cell migration. *Cell Adhes. Migr.* **2013**, *7*, 362–369. [[CrossRef](#)]
48. Kain, K.H.; Klemke, R.L. Inhibition of Cell Migration by Abl Family Tyrosine Kinases through Uncoupling of Crk-CAS Complexes. *J. Biol. Chem.* **2001**, *276*, 16185–16192. [[CrossRef](#)]
49. Hoffman, L.M.; Jensen, C.C.; Chaturvedi, A.; Yoshigi, M.; Beckerle, M.C. Stretch-induced actin remodeling requires targeting of zyxin to stress fibers and recruitment of actin regulators. *Mol. Biol. Cell* **2012**, *23*, 1846–1859. [[CrossRef](#)] [[PubMed](#)]
50. Yi, J.; Kloeker, S.; Jensen, C.C.; Bockholt, S.; Honda, H.; Hirai, H.; Beckerle, M.C. Members of the Zyxin Family of LIM Proteins Interact with Members of the p130Cas Family of Signal Transducers. *J. Biol. Chem.* **2002**, *277*, 9580–9589. [[CrossRef](#)] [[PubMed](#)]
51. Prasad, N.; Topping, R.S.; Decker, S.J. SH2-Containing Inositol 5'-Phosphatase SHIP2 Associates with the p130 Cas Adapter Protein and Regulates Cellular Adhesion and Spreading. *Mol. Cell. Biol.* **2001**, *21*, 1416–1428. [[CrossRef](#)]
52. Li, E.; Stupack, D.G.; Brown, S.L.; Klemke, R.; Schlaepfer, D.D.; Nemerow, G.R. Association of p130CAS with phosphatidylinositol-3-OH kinase mediates adenovirus cell entry. *J. Biol. Chem.* **2000**, *275*, 14729–14735. [[CrossRef](#)]
53. Buday, L.; Wunderlich, L.; Tamás, P. The Nck family of adapter proteins: Regulators of actin cytoskeleton. *Cell. Signal.* **2002**, *14*, 723–731. [[CrossRef](#)]
54. Zhao, C.; Ma, H.; Bossy-Wetzell, E.; Lipton, S.A.; Zhang, Z.; Feng, G.S. GC-GAP, a Rho family GTPase-activating protein that interacts with signalling adapters Gab1 and Gab2. *J. Biol. Chem.* **2003**, *278*, 34641–34653. [[CrossRef](#)] [[PubMed](#)]
55. Rivera, G.M.; Antoku, S.; Gelkop, S.; Shin, N.Y.; Hanks, S.K.; Pawson, T.; Mayer, B.J. Requirement of Nck adaptors for actin dynamics and cell migration stimulated by platelet-derived growth factor B. *Proc. Natl. Acad. Sci. USA* **2006**, *103*, 9536–9541. [[CrossRef](#)]
56. Ngoenkam, J.; Paensuwan, P.; Preechanukul, K.; Khamsri, B.; Yiemiwattana, I.; Beck-García, E.; Minguet, S.; Schamel, W.W.; Pongcharoen, S. Non-overlapping functions of Nck1 and Nck2 adaptor proteins in T cell activation. *Cell Commun. Signal.* **2014**, *12*, 21. [[CrossRef](#)] [[PubMed](#)]
57. Buvall, L.; Rashmi, P.; Lopez-Rivera, E.; Andreeva, S.; Weins, A.; Wallentin, H.; Greka, A.; Mundel, P. Proteasomal degradation of Nck1 but not Nck2 regulates RhoA activation and actin dynamics. *Nat. Commun.* **2013**, *4*, 2863. [[CrossRef](#)]
58. Dikic, I.; Szymkiewicz, I.; Soubeyran, P. Cbl signaling networks in the regulation of cell function. *Cell. Mol. Life Sci.* **2003**, *60*, 1805–1827. [[CrossRef](#)]
59. Howlett, C.J.; Robbins, S.M. Membrane-anchored CBL suppresses HCK protein-tyrosine kinase mediated cellular transformation. *Oncogene* **2002**, *21*, 1707–1716. [[CrossRef](#)]
60. Bureau, J.F.; Cassonnet, P.; Grange, L.; Dessapt, J.; Jones, L.; Demeret, C.; Sakuntabhai, A.; Jacob, Y. The SRC-family tyrosine kinase HCK shapes the landscape of KAP2 interactome. *Oncotarget* **2018**, *9*, 13102–13115. [[CrossRef](#)]
61. Kaabeche, K.; Leminnier, J.; Mee, S.L.; Caverzasio, J.; Marie, P.J. Cbl-mediated degradation of Lyn and Fyn induced by constitutive fibroblast growth factor receptor-2 activation supports osteoblast differentiation. *J. Biol. Chem.* **2004**, *279*, 36259–36267. [[CrossRef](#)]
62. Gonsior, C.; Binamé, F.; Frühbeis, C.; Bauer, N.M.; Hoch-Kraft, P.; Luhmann, H.J.; Trotter, J.; White, R. Oligodendroglial p130Cas Is a Target of Fyn Kinase Involved in Process Formation, Cell Migration and Survival. *PLoS ONE* **2014**, *9*, e89423. [[CrossRef](#)]

63. Hochgraefe, F.; Zhang, L.; O'Toole, S.A.; Browne, B.C.; Pinese, M.; Cubas, A.P.; Lehrbach, G.M.; Croucher, D.; Rickwood, D.; Boulghourjian, A.; et al. Tyrosine Phosphorylation Profiling Reveals the Signaling Network Characteristics of Basal Breast Cancer Cells. *Cancer Res.* **2010**, *70*, 9391–9401. [[CrossRef](#)]
64. Watanabe, S.; Take, H.; Takeda, K.; Yu, Z.X.; Iwata, N.; Kajigaya, S. Characterization of the Cin85 adaptor protein and identification of components involved in CIN85 complexes. *Biochem. Biophys. Res. Commun.* **2000**, *278*, 167–174. [[CrossRef](#)]
65. Verdier, F.; Valovka, T.; Zhyvoloup, A.; Drobot, L.B.; Buchman, V.; Waterfield, M.; Gout, I. Ruk is ubiquitinated but not degraded by the proteasome. *J Biol Chem.* **2002**, *277*, 3402–3408. [[CrossRef](#)] [[PubMed](#)]
66. Maia, V.; Ortiz-Rivero, S.; Sanz, M.; Gutierrez-Berzal, J.; Álvarez-Fernández, I.; Gutierrez-Herrero, S.; De Pereda, J.M.; Porras, A.; Guerrero, C. C3G forms complexes with Bcr-Abl and p38 $\alpha$  MAPK at the focal adhesions in chronic myeloid leukemia cells: Implication in the regulation of leukemic cell adhesion. *Cell Commun. Signal.* **2013**, *11*, 9. [[CrossRef](#)] [[PubMed](#)]
67. Cho, Y.J.; Hemmeryckx, B.; Groffen, J.; Heisterkamp, N. Interaction of Bcr/Abl with C3G, an exchange factor for the small GTPase Rap1, through the adapter protein Crkl. *Biochem. Biophys. Res. Commun.* **2005**, *333*, 1276–1283. [[CrossRef](#)]
68. Kirsch, K.H.; Georgescu, M.M.; Shishido, T.; Langdon, W.Y.; Birge, R.B.; Hanafusa, H. The adapttertype protein CMS/CD2AP binds to the proto-oncogenic protein c-CBL through a tyrosine phosphorylation-regulated Src homology 3 domain interaction. *J. Biol. Chem.* **2001**, *276*, 4957–4963. [[CrossRef](#)] [[PubMed](#)]
69. Kirsch, K.H.; Georgescu, M.M.; Ishimaru, S.; Hanafusa, H. CMS: An adapter molecule involved in cytoskeletal rearrangements. *Proc. Natl. Acad. Sci. USA* **1999**, *96*, 6211–6216. [[CrossRef](#)] [[PubMed](#)]
70. Evans, I.M.; Kennedy, S.A.; Paliashvili, K.; Santra, T.; Yamaji, M.; Lovering, R.C.; Britton, G.; Franke, V.; Kolch, W.; Zachary, I.C. Vascular endothelial growth factor (VEGF) promotes assembly to the p130Cas interactome to drive endothelial chemotactic signalling and angiogenesis. *Mol. Cell. Proteom.* **2017**, *16*, 168–180. [[CrossRef](#)] [[PubMed](#)]
71. Gingras, D.; Michaud, M.; Di Tomasso, G.; Beliveau, E.; Nyalendo, C.; Beliveau, R. Sphingosine-1- phosphate induces the as-ociation of membrane-type 1 matrix metalloproteinase with p130Cas in endothelial cells. *FEBS Lett.* **2008**, *582*, 399–404. [[CrossRef](#)] [[PubMed](#)]
72. Ballestrem, C.; Erez, N.; Kirchner, J.; Kam, Z.; Bershadsky, A.; Geiger, B. Molecular mapping of tyrosine-phosphorylated proteins in focal adhesions using fluorescence resonance energy transfer. *J. Cell Sci.* **2006**, *119*, 866–875. [[CrossRef](#)] [[PubMed](#)]
73. Janoštiak, R.; Tolde, O.; Brůhová, Z.; Novotný, M.; Hanks, S.K.; Rösel, D.; Brábek, J. Tyrosine phosphorylation within the SH3 domain regulates CAS subcellular localization, cell migration, and invasiveness. *Mol. Biol. Cell* **2011**, *22*, 4256–4267. [[CrossRef](#)]
74. Qian, X.; Li, G.; Vass, W.C.; Papageorge, A.; Walker, R.C.; Asnaghi, L.; Steinbach, P.J.; Tosato, G.; Hunter, K.; Lowy, D.R. The Tensin-3 Protein, Including its SH2 Domain, Is Phosphorylated by Src and Contributes to Tumorigenesis and Metastasis. *Cancer Cell* **2009**, *16*, 246–258. [[CrossRef](#)] [[PubMed](#)]
75. Zhang, C.; Miller, D.J.; Guibao, C.D.; Donato, D.M.; Hanks, S.K.; Zheng, J.J. Structural and functional insights into the interaction between the Cas family scaffolding protein p130Cas and the focal adhesion-associated protein paxillin. *J. Biol. Chem.* **2017**, *292*, 18281–18289. [[CrossRef](#)] [[PubMed](#)]
76. McGowan, S.E.; McCoy, D.M. Platelet-derived growth factor receptor- $\alpha$  and Ras-related C3 botulinum toxin substrate-1 regulate mechano-responsiveness of lung fibroblasts. *Am. J. Physiol. Cell. Mol. Physiol.* **2017**, *313*, L1174–L1187. [[CrossRef](#)] [[PubMed](#)]
77. Guzman, M.G.; Dolfi, F.; Russelo, M.; Vuori, K. Cell adhesion regulates the interaction between the docking protein p130cas and 14-3-3 proteins. *J. Biol. Chem.* **1999**, *274*, 5762–5768. [[CrossRef](#)] [[PubMed](#)]
78. Di Stefano, P.; Cabodi, S.; Erba, E.B.; Margaria, V.; Bergatto, E.; Giuffrida, M.G.; Silengo, L.; Tarone, G.; Turco, E.; Defilippi, P. p130Cas-associated Protein (p140Cap) as a New Tyrosine-phosphorylated Protein Involved in Cell Spreading. *Mol. Biol. Cell* **2004**, *15*, 787–800. [[CrossRef](#)]
79. Weissbach, L.; Bernardsb, A.; Herion, D.W. Binding of Myosin Essential Light Chain to the Cytoskeleton-Associated Protein IQGAP. *Biochem. Biophys. Res. Commun.* **1998**, *251*, 269–276. [[CrossRef](#)] [[PubMed](#)]
80. Briggs, M.W.; Sacks, D. IQGAP1 as signal integrator: Ca<sup>2+</sup>, calmodulin, Cdc42 and the cytoskeleton. *FEBS Lett.* **2003**, *542*, 7–11. [[CrossRef](#)]
81. Sit, B.; Gutmann, D.; Iskratsch, T. Costameres, dense plaques and podosomes: The cell matrix adhesions in cardiovascular mechanosensing. *J. Muscle Res. Cell Motil.* **2019**, *40*, 197–209. [[CrossRef](#)]
82. Lee, H.S.; Bellin, R.M.; Walker, D.I.; Patel, B.; Powers, P.; Liu, H.; Garcia-Alareez, B.; de Pereda, J.M.; Liddington, R.C.; Volkman, N.; et al. Characterization of an actin-binding site within the talin FERM do-main. *J. Mol. Biol.* **2004**, *343*, 771–784. [[CrossRef](#)] [[PubMed](#)]
83. Steenblock, C.; Heckel, T.; Czapalla, C.; Santo, A.I.E.; Niehage, C.; Sztacho, M.; Hoflack, B. The Cdc42 Guanine Nucleotide Exchange Factor FGD6 Coordinates Cell Polarity and Endosomal Membrane Recycling in Osteoclasts. *J. Biol. Chem.* **2014**, *289*, 18347–18359. [[CrossRef](#)] [[PubMed](#)]
84. Bauer, T.J.; Gombocz, E.; Krüger, M.; Sahana, J.; Corydon, T.J.; Bauer, J.; Infanger, M.; Grimm, D. Augmenting cancer cell proteomics with cellular images—A semantic approach to understand focal adhesion. *J. Biomed. Inform.* **2019**, *100*, 103320. [[CrossRef](#)] [[PubMed](#)]
85. Takahashi, K.; Suzuki, K. Regulation of protein phosphatase 2A-mediated recruitment of IQGAP1 to beta1 integrin by EGF through activation of Ca<sup>2+</sup>/calmodulin-dependent protein kinase II. *J. Cell. Physiol.* **2006**, *208*, 213–219. [[CrossRef](#)]
86. Leal, M.D.P.C.; Pincini, A.; Tornillo, G.; Fiorito, E.; Bisaro, B.; De Luca, E.; Turco, E.; Defilippi, P.; Cabodi, S. p130Cas Over-Expression Impairs Mammary Branching Morphogenesis in Response to Estrogen and EGF. *PLoS ONE* **2012**, *7*, e49817. [[CrossRef](#)]

87. Cabodi, S.; Moro, L.; Baj, G.; Smeriglio, M.; Di Stefano, P.; Gippone, S.; Surico, N.; Silengo, L.; Turco, E.; Tarone, G.; et al. p130Cas interacts with estrogen receptor  $\alpha$  and modulates non-genomic estrogen signaling in breast cancer cells. *J. Cell Sci.* **2004**, *117*, 1603–1611. [[CrossRef](#)]
88. Okabe, T.; Nakamura, T.; Nishimura, Y.N.; Kohu, K.; Ohwada, S.; Morishita, Y.; Akiyama, T. RICS, a Novel GTPase-activating Protein for Cdc42 and Rac1, Is Involved in the  $\beta$ -Catenin-N-cadherin and N-Methyl-d-aspartate Receptor Signaling. *J. Biol. Chem.* **2003**, *278*, 9920–9927. [[CrossRef](#)]
89. Calautti, E.; Li, J.; Saoncella, S.; Brissette, J.L.; Goetinck, P.F. Phosphoinositide 3-Kinase Signaling to Akt Promotes Keratinocyte Differentiation Versus Death. *J. Biol. Chem.* **2005**, *280*, 32856–32865. [[CrossRef](#)]
90. Lengyel, C.G.; Altuna, S.C.; Habeeb, B.; Trapani, D.; Khan, S.Z.; Lengyel, C.D. The Potential of PI3K/AKT/mTOR Signaling as a Druggable Target for Endometrial and Ovarian Carcinomas. *Curr. Drug Targets* **2020**, *21*, 946–961. [[CrossRef](#)]
91. Nilsson, G.M.A.; Akhtar, N.; Kannius-Jkanson, M.; Baeckström, D. Loss of E-cadherin expression is not a prerequisite for c-erbB2-induced epithelial-mesenchymal transition. *Int. J. Oncol.* **2014**, *45*, 82–94. [[CrossRef](#)]
92. Lo, S.H.; Yu, Q.-C.; Degenstein, L.; Chen, L.B.; Fuchs, E. Progressive Kidney Degeneration in Mice Lacking Tensin. *J. Cell Biol.* **1997**, *136*, 1349–1361. [[CrossRef](#)] [[PubMed](#)]
93. Lefort, C.T.; Wojciechowski, K.; Hocking, D.C. N-cadherin cell-cell adhesion complexes are regulated by fibronectin matrix assembly. *J. Biol. Chem.* **2011**, *286*, 3149–3160. [[CrossRef](#)]
94. Gálvez, B.G.; Matías-Román, S.; Yáñez-Mó, M.; Sánchez-Madrid, F.; Arroyo, A.G. ECM regulates MT1-MMP localization with  $\beta$ 1 or  $\alpha$ v $\beta$ 3 integrins at distinct cell compartments modulating its internalization and activity on human endothelial cells. *J. Biol. Chem.* **2002**, *159*, 509–521. [[CrossRef](#)]
95. Riordan, S.M.; Lidder, S.; Williams, R.; Skouteris, G.G. The beta-subunit of the hepatocyte growth factor/scatter factor (HGF/SF) receptor phosphorylates and associates with CrkII: Expression of CrkII enhances HGF/SF-induced mitogenesis. *Biochem. J.* **2000**, *350*, 925–932. [[CrossRef](#)]
96. Riwaldt, S.; Pietsch, J.; Sickmann, A.; Bauer, J.; Braun, M.; Segerer, J.; Schwarzwälder, A.; Aleshcheva, G.; Corydon, T.J.; Infanger, M.; et al. Identification of proteins involved in inhibition of spheroid formation under microgravity. *Proteomics* **2015**, *15*, 2945–2952. [[CrossRef](#)] [[PubMed](#)]
97. Spisni, E.; Toni, M.; Strillacci, A.; Galleri, G.; Santi, S.; Griffoni, C.; Tomasi, V. Caveolae and caveolae constituents in mechanosensing: Effect of modeled microgravity on cultured human endothelial cells. *Cell. Biochem. Biophys.* **2006**, *46*, 155–164.
98. Shi, F.; Zhao, T.-Z.; Wang, Y.-C.; Cao, X.-S.; Yang, C.-B.; Gao, Y.; Li, C.-F.; Zhao, J.-D.; Zhang, S.; Sun, X.-Q. The Impact of Simulated Weightlessness on Endothelium-Dependent Angiogenesis and the Role of Caveolae/Caveolin-1. *Cell. Physiol. Biochem.* **2016**, *38*, 502–513. [[CrossRef](#)]
99. Saxena, R.; Pan, G.; McDonald, J.M. Osteoblast and Osteoclast Differentiation in Modeled Microgravity. *Ann. N. Y. Acad. Sci.* **2007**, *1116*, 494–498. [[CrossRef](#)]
100. Koaykul, C.; Kim, M.-H.; Kawahara, Y.; Yuge, L.; Kino-Oka, M. Alterations in Nuclear Lamina and the Cytoskeleton of Bone Marrow-Derived Human Mesenchymal Stem Cells Cultured Under Simulated Microgravity Conditions. *Stem Cells Dev.* **2019**, *28*, 1167–1176. [[CrossRef](#)] [[PubMed](#)]
101. Brungs, S.; Kolanus, W.; Hemmersbach, R. Syk phosphorylation—A gravisensitive step in macrophage signalling. *Cell Commun. Signal.* **2015**, *13*, 1–9. [[CrossRef](#)]
102. Dai, Z.; Guo, F.; Wu, F.; Xu, H.; Yang, C.; Li, J.; Liang, P.; Zhang, H.; Qu, L.; Tan, Y.; et al. Integrin  $\alpha$ v $\beta$ 3 mediates the synergetic regulation of core-binding factor  $\alpha$ 1 transcriptional activity by gravity and insulin-like growth factor-1 through phosphoinositide 3-kinase signaling. *Bone* **2014**, *69*, 126–132. [[CrossRef](#)] [[PubMed](#)]
103. Lloyd, S.A.; Lang, C.; Zhang, Y.; Paul, E.M.; Laufenberg, L.J.; Lewis, G.; Donahue, H.J. Interdependence of Muscle Atrophy and Bone Loss Induced by Mechanical Unloading. *J. Bone Miner. Res.* **2014**, *29*, 1118–1130. [[CrossRef](#)] [[PubMed](#)]
104. Bekker-Jensen, D.B.; Kelstrup, C.D.; Batth, T.S.; Larsen, S.C.; Haldrup, C.; Bramsen, J.B.; Sørensen, K.D.; Høyer, S.; Ørntoft, T.F.; Andersen, C.L.; et al. An Optimized Shotgun Strategy for the Rapid Generation of Comprehensive Human Proteomes. *Cell Syst.* **2017**, *4*, 587–599.e4. [[CrossRef](#)]
105. Higashibata, A.; Imamizo-Sato, M.; Seki, M.; Yamazaki, T.; Ishioka, N. Influence of simulated microgravity on the activation of the small GTPase Rho involved in cytoskeletal formation—Molecular cloning and sequencing of bovine leukemia-associated guanine nucleotide exchange factor. *BMC Biochem.* **2006**, *7*, 19. [[CrossRef](#)]
106. Sarkar, S.; Wise, K.C.; Manna, S.K.; Ramesh, V.; Yamauchi, K.; Thomas, R.L.; Wilson, B.L.; Kulkarni, A.D.; Pellis, N.R.; Ramesh, G.T. Activation of activator protein-1 in mouse brain regions exposed to simulated microgravity. *In Vitro Cell Dev. Biol. Anim.* **2006**, *42*, 96–99. [[CrossRef](#)]
107. Ethiraj, P.; Ottinger, A.M.; Singh, T.; Singh, A.; Haire, K.M.; Reddy, S.V. Proteasome inhibition suppress microgravity elevated RANK signaling during osteoclast differentiation. *Cytokine* **2020**, *125*, 154821. [[CrossRef](#)]
108. Koaykul, C.; Kim, M.-H.; Kawahara, Y.; Yuge, L.; Kino-Oka, M. Maintenance of Neurogenic Differentiation Potential in Passaged Bone Marrow-Derived Human Mesenchymal Stem Cells Under Simulated Microgravity Conditions. *Stem Cells Dev.* **2019**, *28*, 1552–1561. [[CrossRef](#)]
109. Lai, Y.-J.; Chen, C.-S.; Lin, W.-C.; Lin, F.-T. c-Src-Mediated Phosphorylation of TRIP6 Regulates Its Function in Lysophosphatidic Acid-Induced Cell Migration. *Mol. Cell. Biol.* **2005**, *25*, 5859–5868. [[CrossRef](#)] [[PubMed](#)]

110. Willier, S.; Butt, E.; Richter, G.H.; Burdach, S.; Grunewald, T.G. Defining the role of TRIP6 in cell physiology and cancer. *Biol. Cell* **2011**, *103*, 573–591. [[CrossRef](#)] [[PubMed](#)]
111. Kopp, S.; Sahana, J.; Islam, T.; Petersen, A.G.; Bauer, J.; Corydon, T.J.; Schulz, H.; Saar, K.; Huebner, N.; Slumstrup, L.; et al. The role of NF $\kappa$ B in spheroid formation of human breast cancer cells cultured on the Random Positioning Machine. *Sci. Rep.* **2018**, *8*, 1–17. [[CrossRef](#)] [[PubMed](#)]
112. Komander, D.; Rape, M. The Ubiquitin Code. *Annu. Rev. Biochem.* **2012**, *81*, 203–229. [[CrossRef](#)] [[PubMed](#)]
113. Li, K.; Zhong, B. Regulation of Cellular Antiviral Signaling by Modifications of Ubiquitin and Ubiquitin-like Molecules. *Immune Netw.* **2018**, *18*, 4. [[CrossRef](#)] [[PubMed](#)]
114. Uchida, T.; Sakashita, Y.; Kitahata, K.; Yamashita, Y.; Tomida, C.; Kimori, Y.; Komatsu, A.; Hirasaka, K.; Ohno, A.; Nakao, R.; et al. Reactive oxygen species upregulate expression of muscle atrophy-associated ubiquitin ligase Cbl-b in rat L6 skeletal muscle cells. *Am. J. Physiol. Physiol.* **2018**, *314*, C721–C731. [[CrossRef](#)] [[PubMed](#)]
115. Nonaka, I. Muscle fiber atrophy. *Rinsho Shinkeigaku* **2012**, *52*, 1315–1317. [[CrossRef](#)] [[PubMed](#)]
116. Sun, Z.; Li, Y.; Zhou, H.; Cai, M.; Liu, J.; Gao, S.; Yang, J.; Tong, L.; Wang, J.; Zhou, S.; et al. Simulated microgravity reduces intracellular-free calcium concentration by inhibiting calcium channels in primary mouse osteoblasts. *J. Cell. Biochem.* **2019**, *120*, 4009–4020. [[CrossRef](#)]
117. Kriegs, B.; Theisen, R.; Schnabl, H. Inositol 1,4,5-trisphosphate and Ran expression during simulated and real microgravity. *Protoplasma* **2006**, *229*, 163–174. [[CrossRef](#)]
118. Bandyopadhyay, C.; Veettil, M.V.; Dutta, S.; Chandran, B. p130Cas Scaffolds the Signalosome to Direct Adaptor-Effector Cross Talk during Kaposi's Sarcoma-Associated Herpesvirus Trafficking in Human Microvascular Dermal Endothelial Cells. *J. Virol.* **2014**, *88*, 13858–13878. [[CrossRef](#)]
119. Zhang, S.; Yuan, M.; Cheng, C.; Xia, D.-H.; Wu, S. Chinese Herbal Medicine Effects on Muscle Atrophy Induced by Simulated Microgravity. *Aerosp. Med. Hum. Perform.* **2018**, *89*, 883–888. [[CrossRef](#)]
120. Hinohara, K.; Kobayashi, S.; Kanauchi, H.; Shimizu, S.; Nishioka, K.; Tsuji, E.; Tada, K.; Umezawa, K.; Mori, M.; Ogawa, T.; et al. ErbB receptor tyrosine kinase/NF- $\kappa$ B signaling controls mammosphere formation in human breast cancer. *Proc. Natl. Acad. Sci. USA* **2012**, *109*, 6584–6589. [[CrossRef](#)]
121. Parsons, M.J.; Patel, P.; Brat, D.J.; Colbert, L.; Vertino, P.M. Silencing of TMS1/ASC Promotes Resistance to Anoikis in Breast Epithelial Cells. *Cancer Res.* **2009**, *69*, 1706–1711. [[CrossRef](#)] [[PubMed](#)]
122. Louis, F.; Deroanne, C.; Nusgens, B.; Vico, L.; Guignandon, A. RhoGTPases as Key Players in Mammalian Cell Adaptation to Microgravity. *BioMed. Res. Int.* **2015**, *2015*, 1–17. [[CrossRef](#)]
123. Kashirini, D.N.; Kononikhin, A.S.; Marina, I.M.; Buravkova, L.B. Secretome of Cultured Human Endothelial Cells in Simulated Microgravity. *Bull. Exp. Biol. Med.* **2019**, *167*, 35–38. [[CrossRef](#)]
124. Deng, B.; Liu, R.; Tian, X.; Han, Z.; Chen, J. Simulated microgravity inhibits the viability and migration of glioma via FAK/RhoA/Rock and FAK/Nek2 signaling. *In Vitro Cell. Dev. Biol. Anim.* **2019**, *55*, 260–271. [[CrossRef](#)]
125. Xue, L.; Li, Y.; Chen, J. Duration of simulated microgravity affects the differentiation of mesenchymal stem cells. *Mol. Med. Rep.* **2017**, *15*, 3011–3018. [[CrossRef](#)] [[PubMed](#)]
126. Tan, X.; Xu, A.; Zhao, T.; Zhao, Q.; Zhang, J.; Fan, C.; Deng, Y.; Freywald, A.; Genth, H.; Xiang, J. Simulated microgravity inhibits cell focal adhesions leading to reduced melanoma cell proliferation and metastasis via FAK/RhoA-regulated mTORC1 and AMPK pathways. *Sci. Rep.* **2018**, *8*, 3769. [[CrossRef](#)] [[PubMed](#)]
127. Zhao, T.; Li, R.; Tan, X.; Zhang, J.; Fan, C.; Zhao, Q.; Deng, Y.; Xu, A.; Lukong, K.E.; Genth, H.; et al. Simulated Microgravity Reduces Focal Adhesions and Alters Cytoskeleton and Nuclear Positioning Leading to Enhanced Apoptosis via Suppressing FAK/RhoA-Mediated mTORC1/NF- $\kappa$ B and ERK1/2 Pathways. *Int. J. Mol. Sci.* **2018**, *19*, 1994. [[CrossRef](#)] [[PubMed](#)]
128. Lin, S.C.; Gou, G.H.; Hsia, C.W.; Ho, C.W.; Huang, K.L.; Wu, Y.F.; Lee, S.Y.; Chen, Y.H. Simulated Microgravity Disrupts Cytoskeleton Organization and Increases Apoptosis of Rat Neural Crest Stem Cells Via Upregulating CXCR4 Expression and RhoA-ROCK1-p38 MAPK-p53. Signaling. *Stem Cells Dev.* **2016**, *25*, 1172–1193. [[CrossRef](#)] [[PubMed](#)]
129. Shi, F.; Wang, Y.C.; Hu, Z.B.; Xu, H.Y.; Sun, J.; Gao, Y.; Li, X.T.; Yang, C.B.; Xie, C.; Li, C.F.; et al. Simulated Microgravity Promotes Angiogenesis through RhoA-Dependent Rearrangement of the Actin Cytoskeleton. *Cell. Physiol. Biochem.* **2017**, *41*, 227–238. [[CrossRef](#)] [[PubMed](#)]
130. Prasad, B.; Grimm, D.; Strauch, S.M.; Erzinger, G.S.; Corydon, T.J.; Lebert, M.; Magnusson, N.E.; Infanger, M.; Richter, P.; Krüger, M. Influence of Microgravity on Apoptosis in Cells, Tissues, and Other Systems In Vivo and In Vitro. *Int. J. Mol. Sci.* **2020**, *21*, 9373. [[CrossRef](#)] [[PubMed](#)]
131. Lin, X.; Zhang, K.; Wei, D.; Tian, Y.; Gao, Y.; Chen, Z.; Qian, A. The Impact of Spaceflight and Simulated Microgravity on Cell Adhesion. *Int. J. Mol. Sci.* **2020**, *21*, 3031. [[CrossRef](#)]
132. Smith, J.K. Osteoclasts and Microgravity. *Life* **2020**, *10*, 207. [[CrossRef](#)]
133. Romswinkel, A.; Infanger, M.; Dietz, C.; Strube, F.; Kraus, A. The Role of C-X-C Chemokine Receptor Type 4 (CXCR4) in Cell Adherence and Spheroid Formation of Human Ewing's Sarcoma Cells under Simulated Microgravity. *Int. J. Mol. Sci.* **2019**, *20*, 6073. [[CrossRef](#)]
134. Ahn, C.B.; Lee, J.H.; Han, G.D.; Kang, H.W.; Lee, S.H.; Lee, J.I.; Son, K.H.; Lee, J.W. Simulated microgravity with floating environment promotes migration of non-small cell lung cancers. *Sci. Rep.* **2019**, *8*, 14553. [[CrossRef](#)]



135. Liao, W.; Elfrink, K.; Bähler, M. Head of Myosin IX Binds Calmodulin and Moves Processively toward the Plus-end of Actin Filaments. *J. Biol. Chem.* **2010**, *285*, 24933–24942. [[CrossRef](#)]
136. Kerber, M.L.; Cheney, R.E. Myosin-X: A MyTH-FERM myosin at the tips of filopodia. *J. Cell. Sci.* **2011**, *124*, 3733–3741. [[CrossRef](#)] [[PubMed](#)]
137. Bauer, J.; Grimm, D.; Hofstaedter, F.; Wieland, W. Techniques for studies on growth characteristics of human prostatic cancer cells. *Biotechnol. Prog.* **1992**, *8*, 494–500. [[CrossRef](#)]
138. Herranz, R.; Anken, R.; Boonstra, J.; Braun, M.; Christianen, P.C.M.; De Geest, M.; Hauslage, J.; Hilbig, R.; Hill, R.J.A.; Lebert, M.; et al. Ground-Based Facilities for Simulation of Microgravity: Organism-Specific Recommendations for Their Use, and Recommended Terminology. *Astrobiology* **2013**, *13*, 1–17. [[CrossRef](#)] [[PubMed](#)]
139. Nassef, M.Z.; Kopp, S.; Wehland, M.; Melnik, D.; Sahana, J.; Krüger, M.; Corydon, T.J.; Oltmann, H.; Schmitz, B.; Schütte, A.; et al. Real Microgravity Influences the Cytoskeleton and Focal Adhesions in Human Breast Cancer Cells. *Int. J. Mol. Sci.* **2019**, *20*, 3156. [[CrossRef](#)]
140. Pang, S.M.; LE, S.; Yan, J. Mechanical responses of the mechanosensitive unstructured domains in cardiac titin. *Biol. Cell* **2018**, *110*, 65–76. [[CrossRef](#)]
141. Grimm, D.; Pietsch, J.; Wehland, M.; Richter, P.; Strauch, S.; Lebert, M.; Magnusson, N.E.; Wise, P.; Bauer, J. The impact of microgravity-based proteomics research. *Expert Rev. Proteom.* **2014**, *11*, 465–476. [[CrossRef](#)] [[PubMed](#)]
142. Nagaraj, N.; Kulak, N.A.; Cox, J.; Neuhauser, N.; Mayr, K.; Hoerning, O.; Vorm, O.; Mann, M. System-wide Perturbation Analysis with Nearly Complete Coverage of the Yeast Proteome by Single-shot Ultra HPLC Runs on a Bench Top Orbitrap. *Mol. Cell. Proteom.* **2012**, *11*, 111. [[CrossRef](#)]
143. Rappsilber, J.; Mann, M.; Ishihama, Y. Protocol for micro-purification, enrichment, pre-fractionation and storage of peptides for proteomics using StageTips. *Nat. Protoc.* **2007**, *2*, 1896–1906. [[CrossRef](#)] [[PubMed](#)]
144. Cox, J.; Mann, M. Max Quant enables high peptide identification rates, individualized p.p.b.-range mass accuracies and proteome-wide protein quantification. *Nat. Biotechnol.* **2008**, *26*, 1367–1372. [[CrossRef](#)] [[PubMed](#)]
145. Cox, J.; Hein, M.; Luber, C.A.; Paron, I.; Nagaraj, N.; Mann, M. Accurate Proteome-wide Label-free Quantification by Delayed Normalization and Maximal Peptide Ratio Extraction, Termed MaxLFQ. *Mol. Cell. Proteom.* **2014**, *13*, 2513–2526. [[CrossRef](#)] [[PubMed](#)]
146. Szklarczyk, D.; Gable, A.L.; Lyon, D.; Junge, A.; Wyder, S.; Huerta-Cepas, J.; Simonovic, M.; Doncheva, N.T.; Morris, J.H.; Bork, P.; et al. STRING v11: Protein–Protein association networks with increased coverage, supporting functional discovery in genome-wide experimental datasets. *Nucleic Acids Res.* **2019**, *47*, D607–D613. [[CrossRef](#)]
147. Breitwieser, F.P.; Colinge, J. IsobarPTM: A software tool for the quantitative analysis of post-translationally modified proteins. *J. Proteom.* **2013**, *90*, 77–84. [[CrossRef](#)]
148. Stanley, R.A.; Gombocz, E.A. System, Method, Software Architecture, and Business Model for Intelligent Object Based Information Platform. U.S. Patent 7,702,639, 20 April 2010.
149. Hancock, W.S.; Wu, S.L.; Stanley, R.R.; Gombocz, E.A. Publishing large proteome datasets: Scientific policy meets emerging technologies. *Trends Biotechnol.* **2002**, *20*, s39–s44. [[CrossRef](#)]
150. Boutet, E.; Lieberherr, D.; Tognolli, M.; Schneider, M.; Bansal, P.; Bridge, A.; Poux, S.; Bougueleret, L.; Xenarios, I.; Boutet, E. UniProtKB/Swiss-Prot, the Manually Annotated Section of the UniProt KnowledgeBase: How to Use the Entry View. *Methods Mol. Biol.* **2016**, *1374*, 23–54. [[CrossRef](#)]
151. Lindberg, D.A. Internet access to the National Library of Medicine. *Eff. Clin. Pr. ECP* **2000**, *3*, 256–260.
152. Milacic, M.; Haw, R.; Rothfels, K.; Wu, G.; Croft, D.; Hermjakob, H.; D’Eustachio, P.; Stein, L. Annotating Cancer Variants and Anti-Cancer Therapeutics in Reactome. *Cancers* **2012**, *4*, 1180–1211. [[CrossRef](#)] [[PubMed](#)]